Quantum criticality, lines of fixed points, and phase separation in doped two-dimensional quantum dimer models

Stefanos Papanikolaou,[1] Erik Luijten,[2] and Eduardo Fradkin[1]
[1]*Department of Physics, University of Illinois at Urbana-Champaign, 1110 West Green Street, Urbana, Illinois 61801-3080, USA*
[2]*Department of Materials Science and Engineering, University of Illinois at Urbana-Champaign, 1304 West Green Street, Urbana, Illinois 61801-2920, USA*
(Received 27 July 2007; published 24 October 2007)

We study phase diagrams of a class of doped quantum dimer models on the square lattice with ground-state wave functions whose amplitudes have the form of the Gibbs weights of a classical doped dimer model. In this dimer model, parallel neighboring dimers have attractive interactions, whereas neighboring holes either do not interact or have a repulsive interaction. We investigate the behavior of this system via analytic methods and by Monte Carlo simulations. At zero doping, we confirm the existence of a Kosterlitz-Thouless transition from a quantum critical phase to a columnar phase. At low hole densities, we find a dimer-hole liquid phase and a columnar phase, separated by a phase boundary which is a line of critical points with varying exponents. We demonstrate that this line ends at a multicritical point where the transition becomes first order and the system phase separates. The first-order transition coexistence curve is shown to become unstable with respect to more complex inhomogeneous phases in the presence of direct hole-hole interactions. We also use a variational approach to determine the spectrum of low-lying density fluctuations in the dimer-hole fluid phase.

DOI: 10.1103/PhysRevB.76.134514 PACS number(s): 74.20.Mn, 05.50.+q, 75.10.−b, 78.20.Bh

I. INTRODUCTION

The behavior of doped Mott insulators is a long-standing open and challenging problem in condensed-matter physics. Mott insulators are the parent states of all strongly correlated electronic systems and as such play a crucial role in our understanding of high-T_c superconductors (HTSC) and many other systems. Their strongly correlated nature implies that their behavior cannot be understood in terms of weakly coupled models. Except for the very special case of one spatial dimension, the physics of doped Mott insulators is currently only understood at a qualitative level. The solution of this challenging problem remains one of the most important directions of research in condensed-matter physics.

Quantum dimer models[1] (QDMs) provide a simplified, and rather crude, description of the physics of a Mott insulator. They provide a correct description of the physics of Mott insulators in regimes in which the spin excitations have a large spin gap. QDMs were proposed originally within the context of the resonating-valence-bond (RVB) mechanism of HTSC.[2,3] These systems are of great interest as they can yield hints on the behavior of more realistic models of quantum frustration.

The main idea behind the formulation of QDMs is that, if the spin gap is large, the spin degrees of freedom become confined in tightly bound singlet states which, in the extreme limit of a very large spin gap, extend only over distance scales of the order of nearest-neighbor sites of the lattice. Thus, in this extreme regime, the Hilbert space can be approximately identified (up to some important caveats[1]) with the coverings of the lattice by valence bonds or dimers.

Surprisingly, even at the level of the oversimplified picture offered by QDMs, the physics of doped Mott insulators remains poorly understood. In this paper, we explore the phase diagrams, and the properties of their phases, of QDMs generalized to include interactions between dimers (or valence bonds) and between dimers and doped (charged) holes. Basic aspects of the physics of these models are reviewed in Ref. 4 and references therein.

Undoped QDMs have been studied more extensively, and by now, they are relatively well understood.[5–11] On bipartite lattices, their ground states show either long-range crystalline valence-bond order of different sorts or are quantum critical,[1,4,8] while on nonbipartite lattices, their ground states are typically disordered and are topological fluids.[7]

The more physically relevant *doped* QDMs, with a finite density of charge carriers (holes), are much less understood, although some properties are known.[12–18] In QDMs, a spin-$\frac{1}{2}$ hole fractionalizes into a bosonic *holon*, an excitation that carries charge but no spin, and a *spinon*, a fermionic excitation that carries spin but no charge.[1,3,4,12] Holons can be regarded as sites that do not belong to any dimer, whereas spinon pairs are broken dimers. This form of electron fractionalization is observable in the spectrum of these systems only in the topological disordered (spin-liquid) phases of the undoped QDM. Otherwise, as in the case of the valence-bond crystalline states which exhibit long-range dimer order, spinons and holons are *confined* and do not exist as independent excitations.[4]

In this paper, we consider several interacting QDMs on a square lattice at finite hole doping and discuss their possible phases and phase transitions as a function of hole density and strength of the interactions. At any finite amount of doping, the system will have a finite density of holes, which are hard-core charged bosons in this description. To simplify the problem, in this work, we do not consider the physical effects of the charge-neutral fermionic spinons which, in principle, should also be present. Thus, at this level of approximation, all spin-carrying excitations are effectively projected out. The remaining degrees of freedom are thus dimers ("spin-singlet valence bonds") and charged hard-core bosonic holes. Already this simplified picture of a strongly correlated system is very nontrivial.

For a certain relation between its coupling constants, known as the Rokhsar-Kivelson (RK) condition,[1] QDM Hamiltonians, both with and without holes, can be written as a sum of projection operators. These RK Hamiltonians are manifestly positive definite operators. For this choice of couplings, the ground-state wave function is a zero-energy state which is known exactly. This *RK wave function* is a local function of the degrees of freedom of the QDM, the local dimer, and hole densities. The quantum-mechanical amplitudes of the RK wave functions turn out to have the same form as the Gibbs weights of a two-dimensional (2D) *classical* dimer problem with a finite density of holes. For the generalized doped QDMs that we consider, the norm of the exact ground-state wave function is equal to the partition function of a system of interacting classical dimers at finite hole density. This mapping to a 2D classical statistical mechanical system, for which there is a wealth of available results and methods, makes this class of problems solvable.[1,7,11,17]

In this work, we will investigate the behavior of doped QDMs which satisfy the RK conditions by studying the correlations encoded in their ground-state wave functions. The phase diagrams of these systems turn out to be quite rich. As we shall see, these simple models can describe many aspects of the physics of interest in strongly correlated systems, including a dimer-hole liquid phase (a Bose-Einstein condensate of holes), valence-bond crystalline states, phase separation, and more general inhomogeneous phases. The undoped version of this system was studied in detail in Ref. 14, where a quantum phase transition was found that was argued to belong to the Kosterlitz-Thouless (KT) universality class, from a critical phase to a columnar state with long-range order. In this paper, we confirm that this is indeed the case. At finite hole density, hitherto available results are limited to the form of the associated RK QDM Hamiltonian[17,18] and numerical results for small systems.

In this work, we employ analytic methods[19–22] combined with advanced classical Monte Carlo (MC) simulations[23,24] to probe the correlations in the doped RK wave functions and investigate the phase diagram and its phase transitions. The methods used here can be readily generalized to the case of nonbipartite lattices, for which a number of important results have been published.[7,25,26] In Sec. II, we describe the construction of two generalized quantum dimer RK Hamiltonians that we used in our study. A similar but independent construction has been presented by Castelnovo *et al.*[17] and by Poilblanc *et al.*[18] The RK wave functions of these generalizations of the quantum dimer model have either a fixed number of holes or a variable number of holes and a fixed-hole fugacity. The ground-state wave functions of both models at their associated RK points correspond to a canonical dimer-monomer system in the canonical and grand-canonical ensembles, respectively. Near the end of the paper, in Sec. VI, we introduce a third Hamiltonian, with an associated RK wave function, to study the effects of hole interactions which compete with phase separation at the first-order transitions that we find for both models.

In Secs. III and IV, we study the correlations and the phase diagram for the ground states encoded in these wave functions by means of an analysis of the equivalent classical statistical system of dimers and holes for the RK Hamiltonians of Sec. II. In Sec. III, we summarize the results of a mean-field theory for both noninteracting and interacting classical dimer models at finite doping. The details of the mean-field theory are presented in Appendix A, where we compute the hole-hole correlation function and derive a qualitative phase diagram as a function of hole density and dimer interaction parameters. The main result of this simple mean-field theory is that the phase diagram at finite hole density contains two phases, a dimer-hole fluid and a columnar dimer solid. The columnar-liquid transition is continuous at weak coupling and turns first order at a tricritical point. Naturally, the critical and tricritical behaviors are not correctly described by the mean-field theory, although the general topology of the phase diagram is correct and, remarkably, even the location of the tricritical point is consistent with what we find in the MC simulations of Sec. V.

In Sec. IV, we present a detailed analytic theory of the critical behavior of interacting classical dimers. Sections IV A and IV B focus on the field-theoretic Coulomb-gas approach for this model at zero and finite doping, respectively. We show that, up to a critical value of a parameter, the undoped RK wave function describes a critical system with continuously varying critical exponents, with a phase transition (belonging to the 2D KT universality class) to a state with long-range columnar order. At finite hole doping, we find a hole-dimer liquid phase (with short-range correlations) and a stable phase with long-range columnar order. At low hole densities, the phase boundary is a line of fixed points with varying exponents ending at a KT-type multicritical point where the transition becomes first order. We present a field-theoretical treatment of this tricritical point and a theory of the evolution of the behavior of the columnar and orientational order parameters and of their susceptibilities along the phase boundary. Past the tricritical point, the system is found to exhibit a strong tendency to phase separation, which we verify in our numerical simulations (Sec. V). In Sec. VI, we consider the effects of direct hole-hole interactions near the first-order phase boundary and discuss one of the many inhomogeneous phases which arise in this regime instead of phase separation.

In Sec. V, we confirm our analytic predictions via extensive classical MC simulations of the generalized RK wave functions. For the study of the line of critical points at low doping, we employ the canonical generalized geometric cluster algorithm (GGCA), whereas the first-order transition is studied via grand-canonical Metropolis-type simulations. The GGCA algorithm enables us to study relatively large systems, up to 400×400, for a range of dopings, $0\leqslant x\leqslant0.06$, and to investigate the finite-size scaling behavior. The accessible range of system sizes should be compared to what can be reached for full quantum models, away from the RK condition, where available methods, such as exact diagonalization and Green's function Monte Carlo, allow the study of only very small systems with few holes.[15,18]

In the undoped case, we confirm the existence of a Kosterlitz-Thouless transition from a line of critical points to an ordered columnar state, as found in the work of Alet *et al.*[14,16] We study the scaling behavior of the columnar and orientational order parameters and of their susceptibilities.

We also use a mapping of the orientational order parameter of the interacting classical dimer model to the staggered polarization operator obtained by Baxter for the six-vertex model[27] to fit our MC data and find an accurate estimate of the KT transition coupling in the undoped case.

At low doping, we study the transition from the dimer-hole fluid phase to the columnar state. We confirm that the scaling dimension of the columnar order-parameter operator is equal to 1/8, as predicted by our analytic results of Sec. IV B. We also present a typical set of data that demonstrates how the scaling dimension of the orientational order-parameter varies, again in agreement with the analytic results of Sec. IV B, and use these results to locate numerically the phase boundary. We then turn to the behavior at larger doping and stronger couplings where the transition becomes first order. We study this regime using grand-canonical Metropolis Monte Carlo simulations. We confirm the first-order nature of the phase transition by means of a careful analysis of the finite-size scaling behavior of the order parameters across the phase boundary and of their susceptibilities. We use these results to locate the phase boundary in the first-order regime as well. In Sec. VI, we use MC simulations to study the effects of a direct hole-hole repulsion which suppresses the effects of phase separation, leading instead to a complex phase diagram of inhomogeneous phases, of which we only study its most commensurate case.

In Sec. VII, we study the elementary quantum excitations of the doped QDMs satisfying the RK condition using the single-mode approximation. We only present the main results and have relegated the details to Appendix B. We find that in the dimer-hole liquid phase, hole and dimer density fluctuations have quadratic dispersions $E(k) \sim k^2$. Thus, this phase should be characterized as a Bose-Einstein condensate of bosonic charged particles (holes), but not really a superfluid, for reasons similar to those of Rokhsar and Kivelson.[1] We summarize our overall conclusions in Sec. VIII.

While this paper was being completed (and refereed), a number of independent studies of aspects of this problem have been published.[16–18] Our results agree with those in these references wherever they overlap, as noted throughout this paper.

II. QUANTUM HAMILTONIANS FOR INTERACTING DIMERS AT FINITE HOLE DENSITY

The Hamiltonian of the quantum dimer model (QDM) can be written in the Rokhsar-Kivelson (RK) form[1] as the sum of a set of mutually noncommuting projection operators Q_p,

$$H = \sum_{\{p\}} Q_p, \tag{2.1}$$

where $\{p\}$ denotes the set of all plaquettes of the square lattice. Each projection operator Q_p acts on the states of the dimers and holes of a plaquette p (or set of plaquettes surrounding p). In the simplest case,[1] each Q_p acts only on the states labeled by the dimer occupation numbers of the links of the plaquette p. In this case, the ground state is described by the short-range RVB wave function[3]

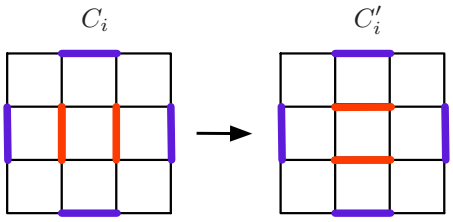

FIG. 1. (Color online) Illustration to clarify the construction of the Hamiltonian (2.3). The central dimer pair is present in all configurations C_i and C_i', whereas the four surrounding dimers may or may not be present. The index i enumerates the 2^4 possible arrangements of the surrounding dimers. The configuration C' differs from the corresponding C by a single flip resonance of the central dimer pair.

$$|\mathrm{RVB}\rangle = \sum_{\{\mathcal{C}\}} |\mathcal{C}\rangle, \tag{2.2}$$

where $\{\mathcal{C}\}$ is the set of (fully packed) dimer coverings of the 2D square lattice and $\{|\mathcal{C}\rangle\}$ is a complete set of orthonormal states. If one regards the dimers as spin-singlet states (with the spins residing on the lattice sites), each configuration represents a set of spin singlets or valence bonds.[2,3] The dimer representation ignores the overcompleteness of the valence-bond singlet states.[1] This problem can be made parametrically small using a number of schemes, including large N approximations[28] and decorated generalizations of the spin-1/2 Hamiltonians.[29]

It is possible and straightforward to generalize the QDM construction so as to include other types of interactions and coverings. In Ref. 11, it was shown how to extend this structure to smoothly interpolate between the square and the triangular lattices. It was also shown there that the same ideas can be used to construct a quantum generalization of the two-dimensional classical Baxter (or eight-vertex) model. In all of these cases, the RK form of this generalized quantum dimer model has an exact ground-state wave function whose amplitudes are equal to the statistical (Gibbs) weights of an associated two-dimensional classical statistical mechanical system on the same lattice. Thus, if the classical problem happens to be a classical critical system, the associated wave function now describes a 2D problem at a quantum critical point. In Ref. 11, such quantum critical points were dubbed "conformal quantum critical points" since the long-distance structure of their *ground-state wave functions* exhibits 2D conformal invariance. Here, we are interested in a different generalization of the QDM in which we consider dimer coverings (although not necessarily fully packed) of the square lattice. We will also consider 2D Hamiltonians whose wave functions correspond to classical interacting 2D dimer problems with local weights. Similar but independent constructions have also been proposed.[17,18,30]

Trying to be as physical and local as possible, we keep the quantum-resonance terms as simple as before (single plaquette moves), but the potential terms (which again have a central plaquette[3]) now have fine-tuned couplings that depend on the nearby plaquettes. Explicitly, we have (cf. Fig. 1)

$$H_d = t\sum_i [-|C_i\rangle\langle C_i'| - |C_i'\rangle\langle C_i| + w^{R_{C_i'}-R_{C_i}}|C_i\rangle\langle C_i| + w^{R_{C_i}-R_{C_i'}}|C_i'\rangle\langle C_i'|], \tag{2.3}$$

where R_{C_i} and $R_{C_i'}$ denote the number of pairs of present dimers formed in configurations C_i and C_i', respectively.

The Hamiltonian of Eq. (2.3) is designed in such a way that it annihilates any superposition of dimer-configuration states which have amplitudes that are of the form w^{N_p}, where w is the parameter appearing in the Hamiltonian and N_p is the number of pairs of neighboring dimers in the configuration.[11] In this sense, the Hamiltonian is a sum of projection operators, and consequently, there is a unique ground state for each topological sector which must be composed of the superposition of these especially weighted configurations. The ground-state wave function $|G\rangle$, the state annihilated by all the projection operators, for this system is

$$|G\rangle = \frac{1}{\sqrt{Z(w^2)}}\sum_{\{\mathcal{C}\}} w^{N_p[\mathcal{C}]}|\mathcal{C}\rangle, \tag{2.4}$$

where $Z(w^2)$, the normalization of this state,

$$Z(w^2) = \sum_{\{\mathcal{C}\}} w^{2N_p[\mathcal{C}]}, \tag{2.5}$$

has the form of the partition function of classically interacting dimers with a coupling $u=-2\ln w$ between parallel neighboring dimers. In the following, we will assume an attractive coupling, $u<0$ or $w>1$. The case $u>0$ was studied for the fully packed case in Ref. 17.

There are two different ways in which we can add doping to our system while still being able to determine the ground state. If we add the following fine-tuned hole-related terms to the initial Hamiltonian (2.3),

$$H^{\text{hole}}_{\text{canonical}} = -t_{\text{hole}}\sum_{<ijk>}\left\{\left[\left|\bullet\ \blacksquare\right\rangle\left\langle\blacksquare\ \bullet\right| + \text{H.c.}\right] - \left|\bullet\ \blacksquare\right\rangle\left\langle\bullet\ \blacksquare\right| - \left|\blacksquare\ \bullet\right\rangle\left\langle\blacksquare\ \bullet\right|\right\}, \tag{2.6}$$

then the resulting ground state becomes

$$|G_{N_h}\rangle = \frac{1}{\sqrt{Z(w^2)}}\sum_{\{\mathcal{C}_{N_h}\}} w^{N_p[\mathcal{C}_{N_h}]}|\mathcal{C}_{N_h}\rangle, \tag{2.7}$$

where the number of holes N_h is now fixed at a specified value. The norm of this wave function, $Z(w^2)$, is the *canonical* partition function for the set of dimer coverings with a fixed number of holes.

On the other hand, if we add the following terms, which do not conserve the number of holes in the system, to the Hamiltonian (2.3),

$$H^{\text{hole}}_{\text{grand-canonical}} = -\tilde{t}_{\text{hole}}\sum_{links}\left\{\left[\left|\ \blacksquare\ \right\rangle\left\langle\ \bullet\ \bullet\ \right| + \text{H.c.}\right] - z^2\left|\ \blacksquare\ \right\rangle\left\langle\ \blacksquare\ \right| - z^{-2}\left|\ \bullet\ \bullet\ \right\rangle\left\langle\ \bullet\ \bullet\ \right|\right\}, \tag{2.8}$$

then the ground state of the system becomes

$$|G\rangle = \frac{1}{\sqrt{Z(w^2,z^2)}}\sum_{\{\mathcal{C}\}} w^{N_p[\mathcal{C}]}z^{N_h[\mathcal{C}]}|\mathcal{C}\rangle, \tag{2.9}$$

with

$$Z(w^2,z^2) = \sum_{\{\mathcal{C}\}} w^{2N_p[\mathcal{C}]}z^{2N_h[\mathcal{C}]}. \tag{2.10}$$

Equation (2.8) includes a natural, short-range repulsion between neighboring holes and an off-diagonal term which represents creation-annihilation of dimers. Furthermore, there is a dimer fugacity term, as in every perturbative derivation of a quantum dimer model.[1] We note that Eq. (2.10) has the same form as a grand-partition function for dimer coverings of the square lattice. This partition function now depends not only on the interaction u defined below [Eq. (2.5)], but also on the hole chemical potential $\mu/|u|=2\ln z$.

Since the canonical and grand-canonical ensembles become equivalent in the thermodynamic limit, the two ground-state wave functions (2.7) and (2.9) must correspond to the same ground-state physics. Furthermore, it is clear that for $w=1$, the models are located at the usual RK point of the quantum dimer model on the square lattice. For a system with periodic boundary conditions, each configuration $\mathcal{C}$ contains only an *even* number of holes, with half of the holes on either sublattice.

We remark that the fact that the exact ground-state wave function is a sum (as opposed to a product) of the ground states of sectors labeled by the number of holes on the lattice is due to the resonance term that we have used to represent the motion of holes. In particular, we have assumed that a dimer can *break* into two holes which themselves repel each other. In the limit of very strong hole-hole repulsions, in strong-coupling perturbation theory, it is straightforward to recover a fixed-hole-density sector with a single-hole resonance move involving three sites in any direction; the coupling strength in Eq. (2.6) then becomes $t_{\text{hole}}\sim z^4\tilde{t}_{\text{hole}}$, and thus, in the limit $z\to 0$, it reduces to an effective hopping amplitude for the holes.

III. MEAN-FIELD RESULTS

To examine the physics described by the ground-state wave functions obtained in the previous section, we start with a discussion of a mean-field theory of the phase diagram. We use the standard approach of regarding the probability densities, obtained by squaring the wave function, as the Gibbs weights of a classical two-dimensional system and focus on the interacting dimer model on the square lattice at finite hole density. Although mean-field theory is insufficient to describe two-dimensional critical systems, it is a useful tool to obtain qualitative features of the phase diagram as

well as the behavior deep in the phases, away from criticality.

The details of this theory are presented in Appendix A. We begin by constructing a Grassmann representation of the partition function for an interacting dimer model using the standard methods introduced by Samuel.[31,32] The resulting theory involves Grassmann (anticommuting) variables residing on the sites of the square lattice. The action of the Grassmann integral is nontrivial and is parametrized by the hole fugacity z and a coupling between dimers $V=z^2(e^u-1)$, where $u=-2\ln w$.

Since the action of the resulting Grassmann path integral is not quadratic in the Grassmann variables, it cannot be reduced to the computation of a determinant. Thus, we use a standard mean-field approach which, in this case, involves the introduction of two Hubbard-Stratonovich (bosonic) fields ϕ_i and χ_{ij}, defined on the sites and links of the square lattice, respectively. Upon integrating out the Grassmann variables, one obtains an effective theory for the fields ϕ_i and χ_{ij} which, as usual, is solved within a saddle-point expansion. The dimer m_0 and hole n densities, as well as the columnar order parameter m, can be expressed straightforwardly in terms of the fields ϕ_i and χ_{ij}. From this effective theory, one can compute an effective potential Γ and the configurations of the observables of interest, n, m_0, and m, as functions of z and V, and determine the phase diagram.

As a function of hole density (or hole fugacity) and u, we find that the phase diagram has two phases (shown qualitatively in Fig. 2), namely, a dimer-hole liquid phase and a hole-poor phase with long-range columnar order. The nature of the transitions between these phases is incorrectly described by the mean-field theory, particularly at zero doping and near the tricritical point. The correct behavior is the subject of a detailed analysis in the subsequent sections. Nevertheless, the mean-field phase diagram correctly predicts that at low hole densities and moderate values of u, the transition between the dimer-hole liquid and the columnar solid phase is continuous; that for large u, the transition is first order; and that there is a tricritical point at

$$u_{tr} \simeq 2.733, \quad z_{tr} \simeq 0.075. \tag{3.1}$$

Remarkably, the Monte Carlo simulations presented in Sec. V yield a tricritical point at a location quite consistent with these values.

Another correct prediction of the mean-field theory is the behavior of the connected hole density correlation function deep in the dimer-hole liquid phase. This prediction, also discussed in detail in Appendix A, fits surprisingly well the Monte Carlo simulations of Krauth and Moessner,[23] performed for a system of classical noninteracting ($u=0$) dimers at finite hole density. The mean-field result is consistent with the simulations for a quite broad region of densities even quite close to the fully packed limit $z\to 0$ where, naturally, a wrong correlation-length exponent is predicted.

IV. PHASE DIAGRAM AND CORRELATIONS FOR INTERACTING DIMERS AND HOLES

We now turn to a more precise analysis of the phase transitions of the interacting classical dimer models as a function of hole density on interaction parameter u. Here, we take advantage of a wealth of information and methods from two-dimensional systems, exact solutions and conformal field theory, to analyze the behavior in detail and extract conclusions that will be quite useful for the analysis of the wave functions. We begin with a discussion of the undoped case and then discuss the physics at finite hole density.

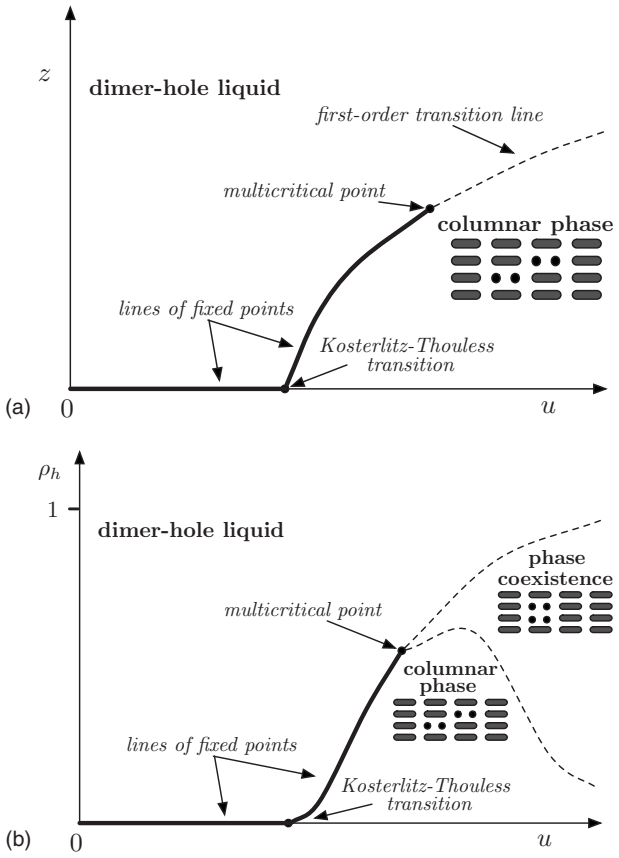

FIG. 2. Qualitative phase diagrams for the interacting doped dimer model. (a) Phase diagram as a function of the fugacity z for the holes and $u=-\ln w$, the dimer interaction coupling constant. The line of continuously varying exponents for low fugacity evolves to a line of first-order transitions. (b) Phase diagram in terms of the hole density ρ_h and the coupling constant u. Here, the line of first-order transitions opens up into a two-phase coexistence region.

A. Interacting dimers at zero hole density

It is a well known fact that both classical and quantum two-dimensional dimer models can be represented in terms of height models. For the classical case, this mapping is well known.[11,33–35] The mapping for the quantum case has also been discussed extensively.[4,9,11,12,36,37] In both cases, the mapping relates each dimer configuration to a configuration of a set of integer-valued (height) variables $h(\vec{r})$, which reside on the sites of the dual lattice, a square lattice in the case of interest here. Thus, this mapping amounts to a duality transformation.

An alternative picture follows from realizing that dimer configurations can be mapped onto the degenerate ground-state configurations of fully frustrated Ising models.[33,38] In

our case, the corresponding spin model is the fully frustrated Ising model on the square lattice (FFSI) at zero temperature. In the Ising model picture, each dimer is dual to an unsatisfied bond of the fully frustrated Ising model and classical dimer interactions correspond to second neighbor interactions in the square lattice FFSI.[39] It is easy to see that holes correspond to unfrustrated plaquettes in the FFSI. In this work, we use primarily the language of the height representation.

To map the square-lattice classical dimer model onto a height model, we follow the prescription given in Ref. 11. One first assigns a height variable to each plaquette. In going around a vertex on the even sublattice clockwise, the height changes by +3 if a dimer is present on the link between the plaquettes and by −1 if no dimer is present on that link. On the odd sublattice, the heights change by −3 and +1, respectively. The dimer constraint that one lattice site belongs to one and only one dimer implies (for the square lattice) that, for the fully packed case, there are four possible configurations of dimers for each lattice site. In the dual height model, this is reproduced by the period 4 property $h \equiv h+4$ of the allowed height configurations. It is easy to see that for the allowed configuration, the average values that the height variables can take at a given site of the direct lattice (a vertex) are $\pm 3/2$ and $\pm 1/2$. On the other hand, a uniform shift of *all* the heights by one unit, $h \to h+1$, leads to an equivalent state. This mapping works strictly speaking only for the fully packed case. Holes are sites that do not belong to any dimer and thus represent violations of the full packing rule. They play the role of topological defects ("vortices") in the (dual) height representation.

The exact solution of the noninteracting fully packed dimer model on the square (and other) lattice has been known for a long time.[40] In particular, the long-distance behaviors of the dimer density correlation functions and the hole density correlation functions are known explicitly.[40,41] These correlation functions obey power-law behaviors and show that this is a critical system. Here, we will use the standard approach to map the exact long-distance behavior of two-dimensional critical systems to the behavior of the simplest critical system, the Gaussian or free boson model.[19] This approach is consistent for the free dimer model on an even lattice with periodic boundary conditions since its central charge (or conformal anomaly) is also $c=1$.

We will use as reference states ("ideal states" in the terminology of Kondev and Henley[42]) the four columnar states of the dimer coverings, which have the largest number of flippable plaquettes, and use them to define an effective field theory for this problem.[9] We will assign a uniform value to the coarse-grained height field $h=0,1,2,3$ to each reference (columnar) state. Let $n_x(\vec{r})$ and $n_y(\vec{y})$ represent the coarse-grained dimer densities of the horizontal link with endpoints at the pairs of lattice sites $\vec{r}$ and $\vec{r}+\vec{e}_x$ and vertical links with endpoints $\vec{r}$ and $\vec{r}+\vec{e}_y$, respectively. Here, $\vec{e}_x$ and $\vec{e}_y$ are two lattice unit vectors along the x and y directions, respectively, with a lattice spacing of 1.

We can now define the columnar local order parameter as the two-component vector,

$$\mathcal{O}_x(x,y) = n_x(x,y) - n_x(x+1,y),$$

$$\mathcal{O}_y(x,y) = n_y(x,y) - n_y(x,y+1), \tag{4.1}$$

which clearly corresponds to the $(\pi,0)$ and $(0,\pi)$ Fourier components of the dimer densities. This two-component order parameter takes four distinct values for each one of the columnar states and changes sign under shifts by one lattice spacing in either direction. It also transforms as a vector under 90° rotations. Thus, it is the order parameter for columnar order.

1. Effective field theory: The noninteracting case

The fluctuations of the free field $h(\vec{r})$ are described by a continuum Gaussian (free boson) model. We will find it simpler to work with the rescaled height field $\phi = \frac{\pi}{2}h$. For this field, the periodicity condition $h \to h+4$ becomes $\phi \to \phi + 2\pi$. (For the rescaled field, the ideal states are $\phi = 0, \pi/2, \pi, 3\pi/2$.) Thus, the allowed operators are 2π periodic functions of ϕ and are either derivatives of ϕ or the exponential (or *charge*) operators $\exp(\pm i\phi)$, $\exp(\pm 2i\phi)$, $\exp(3i\phi)$, and $\exp(\pm 4i\phi)$, which are 2π periodic functions of ϕ.

The action S for the rescaled field is

$$S = \int d^2x \frac{K}{2}(\nabla\phi)^2. \tag{4.2}$$

For the free dimer model, the stiffness is $K = \frac{1}{4\pi}$ (see below).

By matching the exact correlation functions of the free dimer model on the square lattice, one readily finds the following operator identification of the coarse-grained dimer densities in terms of free field operators:[9]

$$n_x - \frac{1}{4} = \frac{1}{2\pi}(-1)^{x+y}\partial_y\phi + \frac{1}{2}[(-1)^x e^{i\phi} + \text{c.c.}], \tag{4.3}$$

$$n_y - \frac{1}{4} = \frac{1}{2\pi}(-1)^{x+y+1}\partial_x\phi + \frac{1}{2}[(-1)^y i e^{i\phi} + \text{c.c.}]. \tag{4.4}$$

In Ref. 9, it was shown that this is an operator identity for the free dimer model on the square lattice in the sense that the asymptotic long-distance behaviors of the dimer density correlation functions computed with this Gaussian model are the same as the exact long-distance correlation functions for the free dimer problem on the square lattice[40,41] provided the stiffness $K = \frac{1}{4\pi}$. Notice that, with this identification, when the field ϕ takes each of the values $0, \pi/2, \pi, 3\pi/2$ (the ideal states), the density operators take four distinct values which reflect the broken symmetries of the four columnar states.

From the operator identification of Eq. (4.4), the columnar order parameter is, up to a normalization constant,

$$\mathcal{O}_x = \cos\phi, \quad \mathcal{O}_y = \sin\phi. \tag{4.5}$$

Due to the effects of dimer-dimer interactions, the form of this effective action is

$$S = \int d^2x \frac{K}{2}(\nabla\phi)^2 + \text{perturbations}. \tag{4.6}$$

The effect of the interactions is a finite renormalization of the stiffness K away from its free dimer value, $K = \frac{1}{4\pi}$.

TABLE I. Scaling dimensions of the order parameters (charge) and hole (vortex) operators at the free dimer point, $K=\frac{1}{4\pi}$, and at the KT point, $K=\frac{2}{\pi}$.

	Columnar $O_{1,0}$	Rotational $O_{2,0}$	$O_{4,0}$	Hole $O_{0,1}$	Hole pair $O_{0,2}$
$K=\frac{1}{4\pi}$	1	4	16	$\frac{1}{4}$	1
$K=\frac{2}{\pi}$	$\frac{1}{8}$	$\frac{1}{2}$	2	2	8

We saw above that, due to the dimer constraints, the allowed charge operators are $O_n(\vec{r})=\exp(in\phi(\vec{r}))$. We also saw that the columnar order parameter is proportional to the operator $\frac{1}{2}(O_1(\vec{r})+O_{-1})(\vec{r})=\cos\phi(\vec{r})$ and carries the unit of charge $n=1$. One can also define *vortex* or *magnetic* operators,[19] and example of which is the hole. A vortex operator causes the field ϕ to wind by $2\pi m$, where m is the vorticity (or *magnetic charge*). One can similarly define a general composite operator $O_{n,m}(\vec{r})$ with n units of (electric) charge and m units of vorticity (or magnetic charge). Its scaling dimensions $\Delta(n,m)$ are[19]

$$\Delta_{n,m}(K)=\frac{n^2}{4\pi K}+\pi K m^2. \tag{4.7}$$

We can now use these results to identify a few operators of interest and give their scaling dimensions. These results are summarized in Table I.

(1) The columnar order parameter is the elementary charge operator $O_{\pm1,0}$ and has no vorticity. On the (columnar) ideal states 0, $\pi/2$, π, and $3\pi/2$, this operator takes the values 1, i, -1, and $-i$, respectively. Its scaling dimension is $\Delta_{1,0}(K)=\frac{1}{4\pi K}$. At the free dimer point, $K=\frac{1}{4\pi}$, its scaling dimension is $\Delta_{1,0}(\frac{1}{4\pi})=1$. This is consistent with the exact results[40,41] that the density correlation function falls off as $1/r^2$. The operator identification of Eq. (4.4) is based on these facts.[9]

(2) The operator $O_{\pm2,0}=\exp(\pm2i\phi)$ takes the values 1, -1, 1, and -1 on each of the ideal columnar states. It is clearly the order parameter for symmetry breaking by 90° rotations: it is the order parameter for *orientational* symmetry.

(3) The operator with the highest allowed electric charge is $O_{\pm4,0}=\exp(\pm4i\phi)$. Its scaling dimension is $\Delta_{4,0}(K)=\frac{4}{\pi K}$. At the free dimer point, it has dimension $\Delta_{4,0}(\frac{1}{4\pi})=16$, and it is a strongly irrelevant operator. This operator arises naturally due to the fact that the microscopic heights h take integer values, and hence height configurations which differ by a uniform integer shift are physically equivalent. This operator does not break any physical symmetry of the dimer model.

(4) The hole operator is represented by the fundamental vortex operator $O_{0,\pm1}$. A vortex with unit positive magnetic charge corresponds to a hole on one sublattice, and a vortex with unit negative magnetic charge to a hole on the other sublattice. The scaling dimension of the vortex (hole) operator is $\Delta_{0,1}(K)=\pi K$. At the free dimer value, the scaling dimension of the hole operator is $\Delta_{0,1}(\frac{1}{4\pi})=\frac{1}{4}$, which is consistent with the exact result that the hole-hole correlation function decays as $1/\sqrt{r}$ at large distances.[40]

(5) The operator which describes a pair of holes on nearby sites of the *same* sublattice is represented by the operators $O_{0,\pm2}$ which carry two units of magnetic charge (vorticity). This operator creates (or destroys) a *diagonal dimer* connecting nearby points on the same sublattice.[5] In the (2+1)-dimensional quantum dimer model, this operator is useful to describe the possible pairing of holes. This operator has dimension $\Delta_{0,2}(K)=4\pi K$. Its scaling dimension at the free dimer point is $\Delta_{0,2}(\frac{1}{4\pi})=1$ and is relevant for $K<\frac{1}{2\pi}$. As noted in Refs. 11 and 25, this operator maps the square lattice into a deformed triangular lattice. The irrelevancy of this operator for $K>\frac{1}{2\pi}$ implies that this line of fixed points also exists for a deformed triangular lattice, as discussed recently in Ref. 26.

(6) The free dimer problem is a free fermion system, which can be solved by Pfaffian methods.[25,31,40] This is actually a theory with two free real (Majorana) fermions or, equivalently, one free complex (Dirac) fermion, at its (massless) fixed point, whose central charge is also $c=1$. The appropriate fermion operator is a composite operator of the order and disorder operators[19,43] which, in this case, is $O_{1/2,1}$. At the free dimer point, the fermion operator has scaling dimension $\Delta_{1/2,1}(\frac{1}{4\pi})=\frac{1}{2}$ and (conformal) spin $nm=\frac{1}{2}$ (as it should for a free fermion). At particular values of K, it is also possible to define parafermion operators[44,45] operators which obey fractional statistics. For instance, at the KT point, $K=\frac{2}{\pi}$ (see below), the operator $O_{1,1/4}$ has dimension $\frac{1}{4}$ and spin $\frac{1}{4}$, and it is a *semion*. In fact, and not surprisingly, a fermionic approach[25] can be used to map this critical line onto an Euclidean version of the Luttinger-Thirring model. The coarse-grained height model description we sue here corresponds to the bosonization approach of the fermionic version of this problem.

2. *Effective field theory: Interactions and phase transition*

We now turn to the effects of dimer-dimer interactions. We recall that we are considering only interactions of a pair of dimers in a plaquette. The interaction energy is

$$H_{\rm int}=-u\sum_{\vec{r}}[n_x(\vec{r})n_x(\vec{r}+\vec{e}_y)+n_y(\vec{r})n_x(\vec{r}+\vec{e}_x)]. \tag{4.8}$$

We wish to find the corresponding operator in terms of the coarse-grained (rescaled) height field ϕ. This can be done by using the operator product expansion (OPE) of the coarse-grained form of the dimer density operators, Eq. (4.4), in terms of the field ϕ. We will also need the standard OPE of the (normal ordered) charge operators[21,46,47]

$$:\cos(n\phi(x)):\cos(n\phi(y)):=\frac{1}{2}:\cos(2n\phi(x)):+\frac{1}{(\mu^2|x-y|^2)^{n^2}}[1-n^2|x-y|^2:(\nabla\phi)^2:+\cdots], \tag{4.9}$$

$$:\sin(n\phi(x))::\sin(n\phi(y)):=$$
$$-\frac{1}{2}:\cos(2n\phi(x)):$$
$$+\frac{1}{(\mu^2|x-y|^2)^{n^2}}[1-n^2|x-y|^2:(\nabla\phi)^2:+\cdots], \tag{4.10}$$

where μ is a short-distance cutoff and the ellipses represent the contributions of irrelevant operators. Using these results, we find that the net effect of the interactions is to renormalize the stiffness K upward,

$$K=\frac{1}{4\pi}+\frac{1}{2}\left(1+\frac{1}{\pi^2}\right)u+\mathcal{O}(u^2), \tag{4.11}$$

where we have denoted $u>0$ for *attractive* interactions. This expression for the renormalization of K is only accurate to linear order in the dimer-dimer interaction. Higher order renormalizations (in u) would result if the effects of irrelevant operators are also taken into account. The relation between K and the microscopic model is nonuniversal and can only be determined either from an exact solution or from a numerical simulation. One can determine the function $K(u)$ from the Monte Carlo simulations we present elsewhere in this paper. What is important is that these nonuniversal effects affect only the relation between the coefficients of the effective theory and not the form of the effective theory itself. Thus, the effective action of the field theory for the interacting classical dimer model at zero hole density has the form

$$S=\int d^2x\left[\frac{K}{2}(\nabla\phi)^2+g\cos(4\phi)\right], \tag{4.12}$$

where we have included the effects of the charge 4 perturbation, $\cos(4\phi)=\cos(2\pi h)$, which biases the coarse-grained height field to take integer values.

For an *anisotropic* dimer-dimer interaction, which arises form a term which weights differently the interactions between parallel horizontal dimers from those of parallel vertical dimers, we would have also found a $\cos(2\phi)$ operator in addition to an anisotropy for the stiffness. Thus, an anisotropy in the dimer-dimer interaction is a relevant perturbation which couples to the orientational order parameter $\cos(2\phi)$.

In Table I, we see that as the attractive interactions grow, there will be a critical value of the interaction u at which the stiffness $K(u_c)=\frac{2}{\pi}$. At this point, the $\cos(4\phi)$ operator has scaling dimension $\Delta_{2,0}=2$, where it becomes marginal. For $u>u_c$ $[K>K(u_c)]$, this operator becomes relevant. We also see that at $K(u_c)=\frac{2}{\pi}$, the columnar order parameter $\cos\phi$ has scaling dimension of 1/8 and it is the most relevant operator in this problem. Thus, this is a phase transition from a *critical phase*, for $K<\frac{2}{\pi}$, without long-range order but with power-law correlations, to a phase with long-range columnar order, for $K>\frac{2}{\pi}$, in which the columnar order parameter has a nonvanishing expectation value. This is a standard Kosterlitz-Thouless (KT) transition[48–50] which is naturally described by the sine-Gordon field theory[51–54] whose (Euclidean) action is given in Eq. (4.12). The only difference between this problem and the standard KT transition, e.g., the classical 2D XY model, is that the phase with a finite-correlation length is ordered: it is a columnar state with a fourfold degenerate nonuniform state, whereas the finite-correlation-length phase of the XY model (and of its dual surface roughening model) has a nondegenerate translation invariant state. In spite of these global differences, this phase transition is in the KT universality class. Thus, the well known behavior of the correlation functions at the KT transition applies to this case as well.[14,16–18] In Sec. V, we verify this behavior by a detailed Monte Carlo study of the columnar and orientational order parameters and of their associated susceptibilities for the interacting dimer model.

B. Interacting dimers at finite hole density

We now consider the dimer model at finite hole density, away from the full packing condition. The classical partition function for this problem is given in Eq. (2.10), where the weights (fugacities) z and w are related to the coupling constant u and the chemical potential μ as described earlier. Recall that the 2D classical partition function $Z(w,z)$ is the norm of the ground-state wave function $|G\rangle$, of Eq. (2.4), of the 2D doped quantum dimer model. In terms of a sum over configurations of electric charges n and magnetic charges (vortices) m, the partition function $Z(w,z)$ is equivalent to that of a generalized (neutral) Coulomb gas (GCG) of electric and magnetic charges in two dimensions,[55,56]

$$Z(w,z)=\sum_{\{n(\vec{r}),m(\vec{R})\}}{}' \exp\left[\frac{N^2}{4\pi K}\sum_{\vec{r},\vec{r}'} n(\vec{r})\ln|\vec{r}-\vec{r}'|n(\vec{r}')\right.$$
$$\left.+\pi K\sum_{\vec{R},\vec{R}'} m(\vec{R})\ln|\vec{R}-\vec{R}'|m(\vec{R}')\right]\exp\left[\sum_{\vec{r}} \ln wn(\vec{r})^2\right.$$
$$\left.+\sum_{\vec{R}} \ln zm(\vec{R})^2-i\sum_{\vec{r},\vec{R}} Nn(\vec{r})m(\vec{R})\Theta(\vec{r}-\vec{R})\right], \tag{4.13}$$

where prime denotes that the sum is restricted to neutral configurations with vanishing total charge and vanishing total vorticity, i.e., $\Sigma_{\vec{r}}n(\vec{r})=\Sigma_{\vec{R}}m(\vec{R})=0$. Here, $\Theta(\vec{r}-\vec{R})$ is the angle between a vortex at $\vec{R}$, as seen from a charge at $\vec{r}$, measured with respect to the (arbitrary) x axis. It is the Cauchy-Riemann dual of the logarithm,

$$G(\vec{r}-\vec{r}')=-\ln|\vec{r}-\vec{r}'|, \tag{4.14}$$

$$\Theta(\vec{r}-\vec{r}')=-\tan^{-1}\left(\frac{y-y'}{x-x'}\right), \tag{4.15}$$

$$-\nabla^2G(\vec{r}-\vec{r}')=2\pi\delta^2(\vec{r}-\vec{r}'), \tag{4.16}$$

$$\partial_\mu G=\epsilon_{\mu\nu}\partial_\nu\Theta. \tag{4.17}$$

As usual, the logarithmic interaction is regularized so that it vanishes for $\vec{r}=\vec{r}'$. The short-distance behavior of the inter-

actions is absorbed in the fugacities z and w.

For the case we are discussing here, the GCG of interest has $N=4$, and Eq. (4.13) is just the Coulomb-gas form of the partition function of the $\mathbb{Z}_4$ model and for the related 2D Ashkin-Teller model. This is a well understood system[21,22,50,52] and in our case, it corresponds to the grand-partition function for the doped interacting dimer model on the square lattice at low hole densities.

In the limit of low fugacities, $z \ll 1$ and $w \ll 1$, the GCG is equivalent to a (generalized) sine-Gordon field theory in two-dimensional Euclidean space-time, whose (Euclidean) Lagrangian is given by[21,52]

$$\mathcal{L}_E = \frac{1}{2}(\partial_\mu \phi)^2 - \frac{2z}{a^2}\cos\left(\frac{N}{\sqrt{K}}\phi\right) - \frac{2w}{a^2}\cos(2\pi\sqrt{K}\tilde{\phi}). \tag{4.18}$$

Here, $\tilde{\phi}$ is the dual field defined by

$$\epsilon_{\mu\nu}\partial_\nu \phi = i\partial_\mu \tilde{\phi}. \tag{4.19}$$

In Eq. (4.18), we can see by inspection that the operators $\cos(\frac{N}{\sqrt{K}}\phi)$ and $\cos(2\pi\sqrt{K}\tilde{\phi})$ can be identified, respectively, with the operators $\frac{1}{2}(O_{N,0}+O_{-N,0})$ and $\frac{1}{2}(O_{0,1}+O_{0,-1})$ discussed above.

We will use this effective field theory to study the transition between the liquid and the ordered phases of the interacting dimer model. At $z=w=0$, this is the KT transition discussed above. For general N, both operators have the scaling dimension if $\frac{N}{\sqrt{K}}=2\pi\sqrt{K}$, i.e., the theory is self-dual, which happens for $K=\frac{N}{2\pi}$. For $N=4$, $K=\frac{2}{\pi}$, both operators have scaling dimension of 2 and both are marginal. This is the only case we will discuss here. (A detailed discussion of the more general case of $N>4$ was given by Lecheminant *et al.*[22])

For $N=4$, the Euclidean Lagrangian becomes[22]

$$\mathcal{L}_E = \frac{1}{2}(\partial_\mu \phi)^2 - \frac{2z}{a^2}\cos(\sqrt{8\pi}\phi) - \frac{2w}{a^2}\cos(\sqrt{8\pi}\tilde{\phi}). \tag{4.20}$$

It turns out that this a problem which can be solved exactly.[20,22] The most direct way of doing this is to perform an analytic continuation from 2D Euclidean space to (1+1)-dimensional Minkowski space-time, i.e., to think of this problem as a (1+1)-dimensional quantum field theory. The *Hamiltonian density* of the equivalent (1+1)-dimensional field theory is

$$\begin{aligned}\mathcal{H} &= \frac{1}{2}(\partial_x \tilde{\phi})^2 + \frac{1}{2}(\partial_x \phi)^2 - \frac{2z}{a^2}\cos(\sqrt{8\pi}\phi) - \frac{2w}{a^2}\cos(\sqrt{8\pi}\tilde{\phi}) \\ &= \frac{1}{2}(\partial_x \tilde{\phi})^2 + \frac{1}{2}(\partial_x \phi)^2 - 2\frac{(z+w)}{a^2}\cos(\sqrt{8\pi}\phi_L)\cos(\sqrt{8\pi}\phi_L) \\ &\quad + 2\frac{(z-w)}{a^2}\sin(\sqrt{8\pi}\phi_L)\sin(\sqrt{8\pi}\phi_L),\end{aligned} \tag{4.21}$$

where we have used the fact that Π, the canonical momentum conjugate to the field ϕ, is simply related to the dual field $\tilde{\phi}$,

$$\Pi = \frac{\delta \mathcal{L}_M}{\delta \phi} = \partial_t \phi = -\partial_x \tilde{\phi}, \tag{4.22}$$

and obey equal-time canonical commutation relations

$$[\phi(x), \Pi(y)] = i\delta(x-y). \tag{4.23}$$

In Eq. (4.21), we used the decomposition of the field ϕ and the dual field $\tilde{\phi}$ into the right and left moving fields ϕ_R and ϕ_L,

$$\begin{aligned}&\phi = \phi_L + \phi_R, \quad \tilde{\phi} = \phi_L - \phi_R, \\ &\phi_L = \frac{1}{2}(\phi + \tilde{\phi}), \quad \phi_R = \frac{1}{2}(\phi - \tilde{\phi}),\end{aligned} \tag{4.24}$$

whose propagators are

$$\begin{aligned}\langle \phi_L(z)\phi_L(w)\rangle &= -\frac{1}{4\pi}\ln(z-w), \\ \langle \phi_R(\bar{z})\phi_R(\bar{w})\rangle &= -\frac{1}{4\pi}\ln(\bar{z}-\bar{w}),\end{aligned} \tag{4.25}$$

where we have used the complex coordinates (not to be confused with the coupling constants) $z=\tau+ix=i(t+x)$ and $\bar{z}=\tau-ix=i(t-x)$, in imaginary and real time, respectively.

It is easy to see[20,22,57] that the following dimension 1 chiral operators,

$$\begin{aligned}J_L^z &= \frac{i}{\sqrt{2\pi}}\partial_z \phi_L, \quad J_L^\pm = \frac{1}{2\pi}{:}e^{\pm i\sqrt{8\pi}\phi_L}{:}, \\ J_R^z &= \frac{-i}{\sqrt{2\pi}}\partial_{\bar{z}} \phi_R, \quad J_R^\pm = \frac{1}{2\pi}e^{\mp i\sqrt{8\pi}\phi_R},\end{aligned} \tag{4.26}$$

with $J_{L,R}^\pm = J_{L,R}^x \pm i J_{L,R}^y$ are the generators of an $\mathrm{su}(2)_1$ Kac-Moody algebra given by the OPE,[22,57]

$$\begin{aligned}J_L^a(z)J_L^b(w) &= \frac{\delta_{ab}}{8\pi^2(z-w)^2} + i\frac{\epsilon_{abc}}{8\pi^2(z-w)}J_L^c(w), \\ J_R^a(\bar{z})J_R^b(\bar{w}) &= \frac{\delta_{ab}}{8\pi^2(\bar{z}-\bar{w})^2} + i\frac{\epsilon_{abc}}{8\pi^2(\bar{z}-\bar{w})}J_R^c(\bar{w}),\end{aligned} \tag{4.27}$$

where $a,b,c=x,y,z$ and ϵ_{abc} is the Levi-Civita tensor. We also note for future use the following operator identifications (still for $K=2/\pi$):

$$\begin{aligned}e^{i\sqrt{8\pi}\phi} &\equiv O_{4,0}, \\ e^{i\sqrt{8\pi}\tilde{\phi}} &\equiv O_{0,1}, \\ J_L^\pm \sim e^{i\sqrt{8\pi}\phi_L} &\equiv O_{\pm 2,\pm 1/2}, \\ J_R^\pm \sim e^{i\sqrt{8\pi}\phi_L} &\equiv O_{\mp 2,\pm 1/2}.\end{aligned} \tag{4.28}$$

The Hamiltonian of Eq. (4.21) can be written in terms of these generators and has the Sugawara form:[57]

$$\mathcal{H} = \frac{2\pi}{3}(\vec{J}_L \cdot \vec{J}_L + \vec{J}_R \cdot \vec{J}_R) - 8\pi^2(z+w)J_L^x J_R^x - 8\pi^2(z-w)J_L^y J_R^y. \tag{4.29}$$

Thus, one recovers the old result[20,51] that at the KT transition, the system has an effective (*dynamical*) SU(2) symmetry.

Given the existence of an $su(2)_1$ symmetry, one expects to find, in addition to the "spin 1" (vector) representation [the su(2) currents], operators associated with the spin-1/2 representation of $su(2)_1$. In the Wess-Zumino-Witten (WZW) version of this theory,[57,58] there is an operator with this property, the field $g(z,\bar{z})$ of the WZW model. This is a 2×2 matrix-valued field with scaling dimension of 1/2. In our theory, we also have an operator with scaling dimension of 1/2, the operator $O_{2,0} \sim \exp(i\sqrt{2\pi}\phi)$ which we saw was related to the order parameter for broken rotational symmetry; see Table I. Thus, the operators of the spin-1/2 (spinor) representation of $su(2)_1$ are identified with the operators

$$g(z,\bar{z}) \sim \begin{pmatrix} e^{-i\sqrt{2\pi}\phi} & e^{-i\sqrt{2\pi}\tilde{\phi}} \\ e^{i\sqrt{2\pi}\phi} & e^{i\sqrt{2\pi}\tilde{\phi}} \end{pmatrix} \sim \begin{pmatrix} O_{-2,0} & O_{0,-1/2} \\ O_{2,0} & O_{0,1/2} \end{pmatrix}. \tag{4.30}$$

Following the approach of Refs. 20 and 22, we will perform a global SU(2) rotation by $\pi/2$ about the y axis which maps $J_{L,R}^x \to J_{L,R}^z$, $J_{L,R}^z \to -J_{L,R}^x$, and $J_{L,R}^y \to J_{L,R}^y$, after which the Hamiltonian becomes

$$\mathcal{H} = \frac{2\pi}{3}(\vec{J}_L \cdot \vec{J}_L + \vec{J}_R \cdot \vec{J}_R) - 8\pi^2(z+w)J_L^z J_R^z - 8\pi^2(z-w)J_L^y J_R^y. \tag{4.31}$$

Once again, one can introduce a new Bose field, which we will call Φ, and its dual $\tilde{\Phi}$ to use the representation of the $su(2)_1$ current algebra of the form of Eq. (4.26). Using that $\partial_z \Phi_L = -i\partial_x \Phi_L$ and $\partial_{\bar{z}} \Phi_R = i\partial_x \Phi_R$, we can rewrite the Hamiltonian as

$$\mathcal{H} = \mathcal{H}_0 + \mathcal{H}_{\text{pert}},$$

$$\mathcal{H}_0 = \frac{1}{2}(\partial_x \Phi)^2 + \frac{1}{2}(\partial_x \tilde{\Phi})^2 - 4\pi(z+w)\partial_x \Phi_L \partial_x \Phi_R,$$

$$\mathcal{H}_{\text{pert}} = -\frac{2(z-w)}{a^2}\sin(\sqrt{8\pi}\Phi_L)\sin(\sqrt{8\pi}\Phi_R). \tag{4.32}$$

Thus, along the phase boundary line $z=w$, the term $\mathcal{H}_{\text{pert}}$ is absent and we see that the effective Hamiltonian $\mathcal{H}_0$ involves only marginal operators.[20,22,50,52]

Similarly, the operators in the spin-1/2 representation transform as an su(2) spinor under a $\pi/2$ rotation about the y axis in $su(2)_1$, leading to the identifications

$$O_{-2,0} \to O_{0,1/2} = e^{i\sqrt{2\pi}\tilde{\Phi}},$$

$$O_{2,0} \to -O_{0,-1/2} = -e^{-i\sqrt{2\pi}\tilde{\Phi}},$$

$$O_{0,-1/2} \to -O_{2,0} = -e^{i\sqrt{2\pi}\Phi},$$

$$O_{0,1/2} \to -O_{-2,0} = -e^{-i\sqrt{2\pi}\Phi}, \tag{4.33}$$

where the operators on the right hand side of Eq. (4.33) are vertex operators written in terms of the new bosons Φ and $\tilde{\Phi}$. Notice that this is a duality transformation.

However, there is an operator in this theory, namely, $O_{\pm 1,0}$, which does not have $su(2)_1$ quantum numbers. As a result, it will have a quite different behavior along the phase boundary. In contrast, all the other operators in this theory carry $su(2)_1$ quantum numbers. [As remarked in Ref. 20, this is not truly an $su(2)_1$ theory, although it contains it, but rather connected with a $\mathbb{Z}_2$ orbifold as well.] It is straightforward to check that the operators $O_{\pm 1,0}$ do not have an OPE with the operators which do transform under $su(2)_1$ (or, rather, that the OPE involves only irrelevant operators). Since the marginal operator which deforms the $su(2)_1$ theory along the phase boundary does transform under $su(2)_1$, the operator $O_{\pm 1,0}$ will not mix (in the sense of its OPE) with the marginal operator either. We will see that this implies that the dimension of this operator remains equal to 1/4 along the entire line, a result that is also well known (see, for instance, Ref. 59.) In contrast, the operators of the spin-1/2 representation, Eq. (4.30), do transform under $su(2)_1$, a fact which is generated by their OPEs with the $su(2)_1$ generators,[57] and we will now see that their scaling dimensions do change along the phase boundary line. In Sec. V, we present evidence from Monte Carlo simulations in support of both statements.

We can now use this approach to solve this problem exactly along the phase boundary. Formally, the Hamiltonian $\mathcal{H}_0$ of Eq. (4.32) is equivalent to a spinless Luttinger model with attractive backscattering interactions.[60] As in the case of the Luttinger model, the problem is solved by means of a Bogoliubov transformation of the right and left moving bosons. This procedure breaks the $su(2)_1$ symmetry explicitly. We introduce a new bose field χ and its dual field $\tilde{\chi}$. The left and right moving components of these fields, χ_L and χ_R, are linearly related to the left and right moving fields Φ_L and Φ_R by

$$\chi_L = \frac{1}{2}\left(\sqrt{\kappa} + \frac{1}{\sqrt{\kappa}}\right)\Phi_L + \frac{1}{2}\left(\frac{1}{\sqrt{\kappa}} - \sqrt{\kappa}\right)\Phi_R,$$

$$\chi_R = \frac{1}{2}\left(\frac{1}{\sqrt{\kappa}} - \sqrt{\kappa}\right)\Phi_L + \frac{1}{2}\left(\sqrt{\kappa} + \frac{1}{\sqrt{\kappa}}\right)\Phi_R, \tag{4.34}$$

where κ is given by

$$\kappa = \sqrt{\frac{1+2\pi(z+w)}{1-2\pi(z+w)}}. \tag{4.35}$$

The inverse transformation of Eq. (4.34), which relates Φ_L and Φ_R to χ_L and χ_R, has the same form and it is obtained simply by replacing κ by $1/\kappa$.

The Hamiltonian $\mathcal{H}_0$ in terms of the new fields becomes

$$\mathcal{H}_0 = \frac{v}{2}[(\partial_x \tilde{\chi})^2 + (\partial_x \chi)^2], \tag{4.36}$$

where the "dimensionless velocity" v is

$$v = \sqrt{1 - 4\pi^2 (z+w)^2}, \tag{4.37}$$

which can be absorbed in a suitable rescaling of the x coordinate, $x \to x\sqrt{v}$. Notice that the parameter κ plays the same role as the stiffness K defined above, which governed the change of the scaling dimensions at zero doping. Similarly, κ governs the change of the scaling dimensions along the $z=w$ phase boundary of the systems at finite hole density. Here too, the relationship between this stiffness κ and the microscopic interactions is nonuniversal, and the validity of Eqs. (4.35) and (4.37) is restricted to the weak-coupling regime in which this continuum theory holds. Notice that, since $z \geqslant 0$ and $w \geqslant 0$, we will always have $\kappa \geqslant 1$. This fact will play an important role below.

We can now use these results to determine the scaling dimension of the perturbation $\mathcal{H}_{\text{pert}}$ along the phase boundary. It is straightforward to write the perturbation $\mathcal{H}_{\text{pert}}$ in terms of the new field χ and its dual $\tilde{\chi}$:

$$\begin{aligned}\mathcal{H}_{\text{pert}} &= -\frac{2(z-w)}{a^2} \sin(\sqrt{8\pi}\Phi_L)\sin(\sqrt{8\pi}\Phi_R) \\ &= \frac{(z-w)}{a^2}\left[\cos(\sqrt{8\pi\kappa}\chi) - \cos\left(\sqrt{\frac{8\pi}{\kappa}}\tilde{\chi}\right)\right].\end{aligned} \tag{4.38}$$

C. Critical behavior along the phase boundary

1. Correlation-length exponent

From Eq. (4.38), we find that the operator which perturbs the line of fixed points along the phase boundary at finite density, $\mathcal{H}_{\text{perp}}$, involves two operators whose scaling dimensions are $2\kappa > 2$ and $\frac{2}{\kappa} < 2$, respectively, since $\kappa > 1$. Thus, this operator becomes more relevant along the phase boundary, away from the KT point, which in this language has $\kappa = 1$. In fact, if we neglect the effects of the irrelevant operator (which is a safe thing to do only away from the KT point since its only important effect is a finite renormalization of κ), we see that the effective theory in the vicinity of the phase boundary is a sine-Gordon theory for the dual field $\tilde{\chi}$. Since the scaling dimension of the relevant operator is $2/\kappa$, it follows that, away from the KT point, the correlation length ξ diverges as the phase boundary is approached as

$$\xi \sim |z-w|^{-\nu}, \quad \nu = \frac{1}{2 - \frac{2}{\kappa}} = \frac{\kappa}{2(\kappa-1)}. \tag{4.39}$$

Thus, the correlation-length exponent decreases (from infinity) along the phase boundary away from the KT point. It is apparent from the form of the perturbation that away from the KT point, there is simple scaling, up to contributions of strictly irrelevant operators. On the other hand, as $\kappa \to 1$, the relevant operator becomes marginally relevant and the irrelevant operator becomes marginally irrelevant. Thus, as $\kappa \to 1$, we should expect logarithmic corrections to scaling and a complex crossover near $\kappa = 1$.

2. Columnar order parameter and its susceptibility

On the other hand, we noted above that the dimension of the columnar order parameter operator $\frac{1}{2}(O_{1,0} + O_{-1,0})$ remains fixed at the KT value of $\Delta_{1,0} = 1/8$. Hence, for this operator, we find $\eta_{1,0} = 1/4$. On the other hand, from scaling, we know that the susceptibility exponent obeys the scaling relation $\gamma_{1,0} = (2-\eta)\nu$, where ν is given by Eq. (4.39). Hence,

$$\gamma_{1,0} = \frac{7\kappa}{8(\kappa-1)} \tag{4.40}$$

is the susceptibility exponent of the columnar order parameter, which also increases along the phase boundary, even though $\gamma_{1,0}/\nu = 7/4$ along the whole phase boundary (provided the transition remains continuous).

3. The orientational order parameter and its susceptibility

We can use the operator identifications to look at the behavior of the orientational order parameter which we saw above is the operator $O_{2,0}$ of the original version of the theory. We also saw that this operator is a component of the spin-1/2 representation of $\text{su}(2)_2$. We also found how it transforms. In particular, we have

$$O_{\pm 2,0} \to \mp e^{\mp i\sqrt{2\pi/\kappa}\tilde{\chi}}. \tag{4.41}$$

Along the phase boundary, the scaling dimension of this operator is

$$\Delta_{2,0} = \frac{1}{2\kappa} < \frac{1}{2}, \tag{4.42}$$

which it is always relevant, and

$$\eta_{2,0} = \frac{1}{\kappa}. \tag{4.43}$$

Using once again the scaling relation $\gamma_{2,0} = (2-\eta_{2,0})\nu$, we find that the susceptibility exponent for the orientational order parameter is

$$\gamma_{2,0} = \frac{2\kappa - 1}{2(\kappa-1)}, \tag{4.44}$$

which also decreases along the phase boundary away from the KT point.

D. Tricritical point, first-order transition, and phase separation

Let us now discuss how this critical line turns into a first-order transition at a multicritical point. In Secs. V and V D, we use Monte Carlo simulations to show that this is indeed what happens. In Sec. IV B, we used mean-field methods which indicated that the transition eventually should become first order. For this to work, we should be able to predict the

existence of a tricritical point along the phase boundary at which the transition becomes first order. It turns out that this is the case and that the first-order transition is triggered by an effective attractive interaction between holes on the same sublattice, leading to phase separation.

To see how this happens, we need to discuss the effects of irrelevant operators along the phase boundary. As we stated above, their most important effect is a finite and nonuniversal renormalization of κ away from the value given in Eq. (4.35). We have also focused on the role of the operators $O_{4,0}$ and $O_{0,1}$ as they are both marginal at the KT transition. However, we also saw that one combination of these two operators remains marginal along the phase boundary and its coupling constant determines the value of κ, through Eq. (4.35). On the other hand, the other combination is the sum of a relevant operator, $\cos(\sqrt{(8\pi/\kappa)}\tilde{\chi})$ with scaling dimension of $2/\kappa$, and of an irrelevant operator, $\cos(\sqrt{8\pi\kappa}\chi)$ with scaling dimension of 2κ. The dimension of the irrelevant operator increases along the phase boundary (thus becoming more irrelevant), while the dimension of the relevant operator decreases as κ increases (thus becoming more relevant.)

One possible scenario for a first-order transition is found by noting that as $\kappa\to\infty$, the dimension of the relevant operator vanishes, and the "thermal eigenvalue" $\gamma_{0,1}/\nu\to 2$. Thus, at this point, naturally, provided this limit is accessible, the line of fixed points reaches a discontinuity fixed point[61] and the transition becomes first order. However, at this point, the theory becomes pathological (as $\kappa\to\infty$, $v\to 0$) and one may suspect that other physical effects, contained in irrelevant operators, may intervene before this happens.

We have so far neglected other operators which are even more irrelevant at the KT transition. For example, the operators $O_{8,0}$ and $O_{0,2}$ have dimension of 8 at the KT point. Recall that the operator $O_{0,2}$ represents pairs of holes on the *same sublattice*. Both of these operators are present in any lattice problem (such as the interacting dimer model) and play no significant role at the KT transition (beyond a nonuniversal but otherwise trivial shift of the critical coupling), and for this reason, they were (correctly) neglected. However, along the phase boundary, the scaling dimensions of these operators change. Using the OPE, it is easy to see that along the phase boundary, both operators contain the operators (among others which are less important) $O_{0,2}\sim\cos(2\sqrt{(8\pi/\kappa)}\tilde{\chi})$ with scaling dimension of $8/\kappa$ and $O_{8,0}\sim\cos(2\sqrt{8\pi\kappa}\chi)$ with scaling dimension of 8κ. Even though they are not explicitly present in our starting theory, these operators will be generated under renormalization, and close enough to the KT point, $\kappa\gtrsim 1$, they both are and remain irrelevant.

However, although κ also changes in a nonuniversal manner, the dependence of the dimensions with κ does not, as it follows from the structure of the theory. Thus, provided the dependence between κ and the microscopic couplings allows it, it may be possible to reach a point along the phase boundary at which $\kappa=4$. This will happen at a critical value of the coupling constant u and a critical value of the hole density ρ [or, equivalently, at a critical value of the hole fugacity z (cf. Fig. 2)].

At this critical value of κ, the scaling dimension of the operators $O_{0,2}$ becomes equal to 2, and together with the strictly marginal operator $O_{4,0}$, there are now two marginal operators at this point. Thus, the system is at a *tricritical* point at this value of the parameters.[62] Past this point, $O_{0,2}$ becomes marginally relevant along the phase boundary. In this regime, the effective field theory at the phase boundary is a sine-Gordon theory for the field $\tilde{\chi}$ with the marginally relevant operator $O_{0,2}$. Since the sine-Gordon theory in this regime is massive, it has a finite-correlation length, and since $O_{0,2}$ is marginally relevant, the correlation length along the phase boundary, which has now become a coexistence curve, has an essential singularity as a function of the distance to the tricritical point, i.e., a KT-like transition. Thus, the transition becomes *first order* along the phase boundary past the tricritical point with a correlation length that scales like $\xi\sim e^{\text{const}/\sqrt{s}}$, where s is the distance to the tricritical point measured along the coexistence curve. In contrast, the correlation length across the phase boundary (below the tricritical point) exhibits conventional power-law scaling. Closely related scenarios for the existence of such tricritical points have been suggested in other systems, such as the extended Hubbard model in one dimension,[63] the two-dimensional classical Ashkin-Teller model,[64,65] and the dilute four-state Potts model,[66] which is a statistical system with very similar phase diagram.

What happens as the tricritical point is reached can be understood more physically by noting that at that point, the operator $O_{0,2}$, which measures the probability amplitude for a pair of holes (on the same sublattice), becomes relevant. The relevance of $O_{0,2}$ indicates that holes on the same sublattice now have a strong effective attractive interaction and have a strong tendency to pairing and consequently phase separate. The effective field theory description given above corresponds to the grand-canonical picture, since the coupling constants are simple functions of the hole fugacity. On the other hand, in the canonical description, i.e., at fixed-hole density ρ, the coexistence curve opens up into a two-phase region: there is phase separation between hole-poor regions with local columnar dimer order and hole-rich regions. The jump in the hole and dimer densities (as well as in the order parameters) across the first-order transition is governed by the correlation length at the coexistence curve. Thus, close to the tricritical point, the jump in the densities (i.e., the width in density of the two-phase region) has the scaling form $\Delta\rho\sim\xi^{-2}$ and therefore vanishes with an essential singularity as the tricritical point is approached. Similar scaling behavior applies to the discontinuity of the columnar and orientational order parameters across the two-phase region.

In the subsequent sections, we will give further evidence for the nature of the phase transitions in this system, including the first-order transition, using Monte Carlo simulations in the canonical and grand-canonical ensembles.

V. MONTE CARLO SIMULATIONS

We now employ Monte Carlo simulations to map out the phase diagram of the doped quantum dimer models at their generalized RK points. This approach is complementary to the analytic approach of Secs. III, IV A, and IV B and of Appendix A. We first introduce (Sec. V A) a canonical

Monte Carlo algorithm for interacting dimers. In Sec. V B, we apply this method to the case of the interacting fully packed classical dimer model on the square lattice, a system that has been studied recently in some detail,[14,16–18] and study its phase transition. In Secs. V C and V D, we consider the case of the doped dimer model at low doping and map out the critical line, verifying the theoretical scenario discussed in Sec. IV B. In Sec. V D, we combine the cluster algorithm with conventional grand-canonical moves that permit us to determine the first-order transition line as a function of dimer fugacity z_d and interaction strength u. We also estimate the location of the multicritical point discussed in Appendix A and Sec. IV B using data from both canonical and grand-canonical simulations.

A. Algorithm for classical interacting dimers

At high dimer coverage (low doping), conventional Monte Carlo algorithms become very inefficient. On the other hand, in Ref. 23, it was demonstrated that a geometric cluster algorithm (GCA) can work efficiently for dimers that only have a repulsive hard-core interaction. We briefly summarize this algorithm here. The overlap of two hard-core dimer configurations generates a transition graph. This graph consists of disjoint subgraphs of dimers alternating between the two configurations. In the presence of holes, there are two possible types of graphs: an *open graph*, which always terminates on a hole, or a *closed loop*. Any Monte Carlo move corresponds to a transition graph of the initial and final configurations. In the geometric cluster algorithm, the two subgraphs are related by a global lattice symmetry. The algorithm obtains long transition graphs with minimal overhead: moves are never rejected, and each dimer encountered during the construction of the graph participates in the move. The construction proceeds as follows.[23] First, a "seed" dimer and a symmetry axis are chosen at random. The seed dimer is reflected with respect to the symmetry axis, and if it overlaps with other dimers, these are reflected as well. This proceeds in an iterative fashion until there are no more dimer overlaps or, equivalently, when an open or closed graph has been formed. On the square lattice, the algorithm is ergodic if we allow both diagonal and horizontal-vertical axes passing through sites of the lattice. The first choice allows changing the numbers of horizontal and vertical dimers, whereas the second one permits moving through the different winding number sectors. Transition graphs generated by the algorithm are symmetric with respect to the symmetry axis and cross it at most twice.

We now extend this approach to dimers with additional interactions by exploiting the *generalized* geometric cluster algorithm proposed by Liu and Luijten.[24,67] Now, in a single cluster move, multiple transition graphs and/or open graphs are formed simultaneously while retaining the rejection-free character of the algorithm. This is achieved by also reflecting dimers that do *not* overlap, with a probability that depends on the dimer-dimer coupling. When a dimer i, located at $\vec{r}_i^{\,\mathrm{old}}$, is reflected to a new position $\vec{r}_i^{\,\mathrm{new}}$, there are two classes of dimers that interact with dimer i: (a) dimers which interact with it *before* it is reflected and (b) dimers which interact with i *after* it is reflected. Dimers j, located at positions $\vec{r}_j$, that belong to any of the two classes are included in the cluster (i.e., will be reflected with respect to the symmetry axis) with a probability

$$p_{ij} = \max[1 - e^{-\delta \mathcal{U}_{ij}/k_B T}, 0], \tag{5.1}$$

where $\delta \mathcal{U}_{ij} = V(|\vec{r}_i^{\,\mathrm{new}} - \vec{r}_j|) - V(|\vec{r}_i^{\,\mathrm{old}} - \vec{r}_j|)$ and $V(r)$ represents the interaction between two dimers at a separation r. Thus, the cluster addition probability for dimer j depends *solely* on the energy difference corresponding to a change in relative position of i and j. In the limit of a pure hard-core repulsion, this generalized geometric cluster algorithm reduces to the original GCA.

The GGCA applies only to simulations in the canonical ensemble. To perform Monte Carlo simulations in the grand-canonical ensemble, we alternate the cluster moves with conventional grand-canonical Metropolis moves, consisting of insertion and deletion attempts of single dimers.

B. Zero doping: Kosterlitz-Thouless transition to a columnar valence-bond crystal

According to the theoretical study of Sec. IV A and also from the results of Refs. 14, 16, and 17, we expect to find a Kosterlitz-Thouless transition at zero doping as a function of the dimer interaction. To detect and locate this transition, we exploit the fact that there is an ordered phase in the large-u region and define columnar and orientational order parameters,

$$C(\mathbf{r}) \equiv \sum_{i=x,y} [n_i(\mathbf{r}) - n_i(\mathbf{r} + \mathbf{e}_i)], \tag{5.2}$$

$$R(\mathbf{r}) \equiv n_x(\mathbf{r}) n_x(\mathbf{r} + \mathbf{e}_y) - n_y(\mathbf{r}) n_y(\mathbf{r} + \mathbf{e}_x), \tag{5.3}$$

where $n_i(\mathbf{r})$ denotes the dimer density at $\mathbf{r}$. $\langle C(\mathbf{r}) \rangle$ is nonvanishing only in a columnar-ordered phase, providing a signature of translational symmetry breaking (with a fourfold degeneracy), whereas $\langle R(\mathbf{r}) \rangle$ measures the breaking of invariance under $\pi/2$ rotations. In terms of the most relevant operators of the effective theory of Sec. IV A, using OPE, we make the following identifications:

$$C \sim \frac{1}{2}(O_{1,0} + O_{-1,0}), \tag{5.4}$$

$$R \sim \frac{1}{2}(O_{2,0} + O_{-2,0}). \tag{5.5}$$

Having a proper correspondence between the effective theory described in Sec. IV A and the microscopic order parameters (5.3), we may verify our predictions. Since the conventional fourth-moment ratio (directly related to the Binder cumulant[68]) of the order parameter generally does not show a well-defined crossing at a KT transition, we instead use a scaling function of the form of the spontaneous staggered polarization of the six-vertex model,[27] which maps on the same vertex operator as R in the Coulomb-gas representation and is in the same universality class. Keeping only the most relevant terms, this function has the form

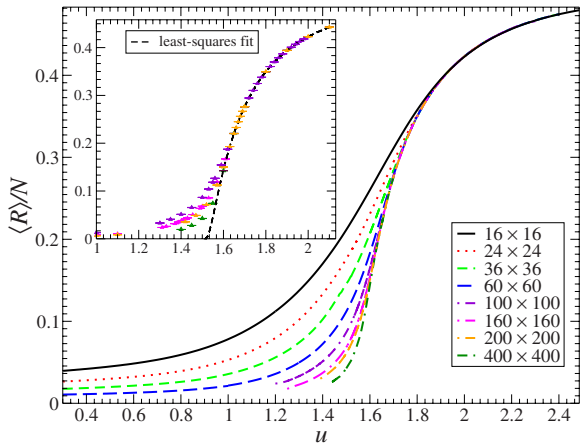

FIG. 3. (Color online) The orientational order parameter R in the undoped case: it vanishes for $u<u_c$ and has an essential singularity at u_c. The curves represent Monte Carlo data for different lattice sizes, interpolated via multiple histogram reweighting. Inset: data collapse, with a least-squares fit to the exact scaling function for the staggered polarization operator of the six-vertex model (5.6) related to R by a universality mapping as discussed in the text.

$$\langle R(u)\rangle = \left(a\frac{1}{\sqrt{u-u_c}}+\cdots\right)e^{[-c/\sqrt{u-u_c}+d\sqrt{u-u_c}+\cdots]}. \quad (5.6)$$

From a careful nonlinear least-squares fit to the numerical data outside the finite-size regime (cf. Fig. 3), we obtain $u_c = 1.508 \pm 0.003$.

For completeness, we also investigate the behavior of the fourth-order amplitude ratios $Q_M = \langle M^2\rangle^2/\langle M\rangle^4$ with $M=C$, R. The behavior of Q_C, shown in Fig. 4, is similar to what is expected for the XY model, namely, a collapse of all curves in the critical low-u phase and no well-defined crossing of curves for different system sizes. In contrast, Q_R (Fig. 5) is found to exhibit such strong finite-size effects in the critical phase that its behavior almost resembles that of a regular

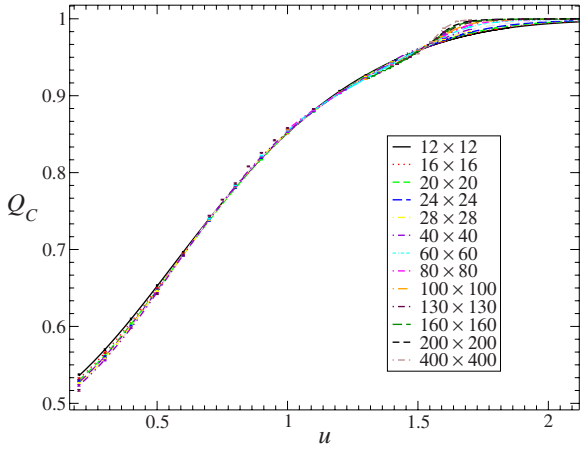

FIG. 4. (Color online) Fourth-order amplitude ratio of the columnar order parameter C in the undoped case. The curves for all system sizes essentially coincide for the entire critical phase ($u<u_C$), as expected for a KT transition.

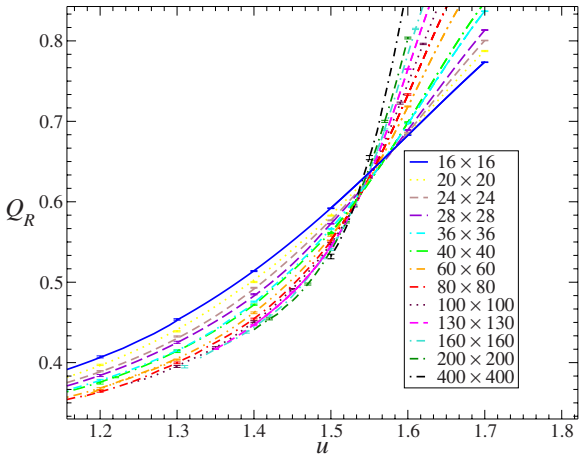

FIG. 5. (Color online) Fourth-order amplitude ratio of the orientational order parameter R in the undoped case. In contrast to the amplitude ratio of the columnar order parameter C (Fig. 4), this quantity exhibits a strong finite-size dependence, leading to an effective crossing point that can be used to locate the transition point.

continuous phase transition. This anomalous behavior explains why the crossing point of the curves for different system sizes could be exploited to obtain an accurate estimate of the critical coupling.[14,16] In the figures presented in this section, the multiple histogram reweighting method[69] has been used to interpolate all data obtained at different values for the coupling parameter. This allows us to accurately locate crossing points and extrema in the curves.

Alet *et al.*[14,16] and Poilblanc *et al.*[18] used transfer-matrix calculations and Monte Carlo simulations to study the critical behavior of the undoped system for $u>0$ (attractive dimer interactions), whereas Castelnovo *et al.*[17] used transfer-matrix methods to study primarily the $u<0$ ("repulsive") regime. In addition, in Ref. 16, the doped interacting dimer model was also briefly studied for low doping by means of numerical transfer-matrix techniques. All these results are consistent and complementary to those presented in the following section.

C. Low doping: Line of fixed points

We now proceed to the low-doping regime. We perform simulations in the canonical ensemble for couplings near the critical region and for hole densities $\rho_h = 0.004, 0.01, 0.02, 0.04, 0.06$. Figure 6 shows, for $\rho_h = 0.06$, the susceptibilities of the columnar and orientational order parameters, C and R, followed by the corresponding fourth-order amplitude ratios in Fig. 7.

According to the predictions of Sec. IV B, we expect that the columnar order parameter C, which maps onto the $O_{1,0}$ effective operator in the scaling limit, will retain its scaling dimension of $1/8$ along the critical line that emerges from the KT transition point for low hole doping and which constitutes the phase boundary between the dimer-hole liquid and the columnar solid phases. This constant value of the scaling dimension of C is the most salient signature of this critical line: The scaling dimensions of all the other operators

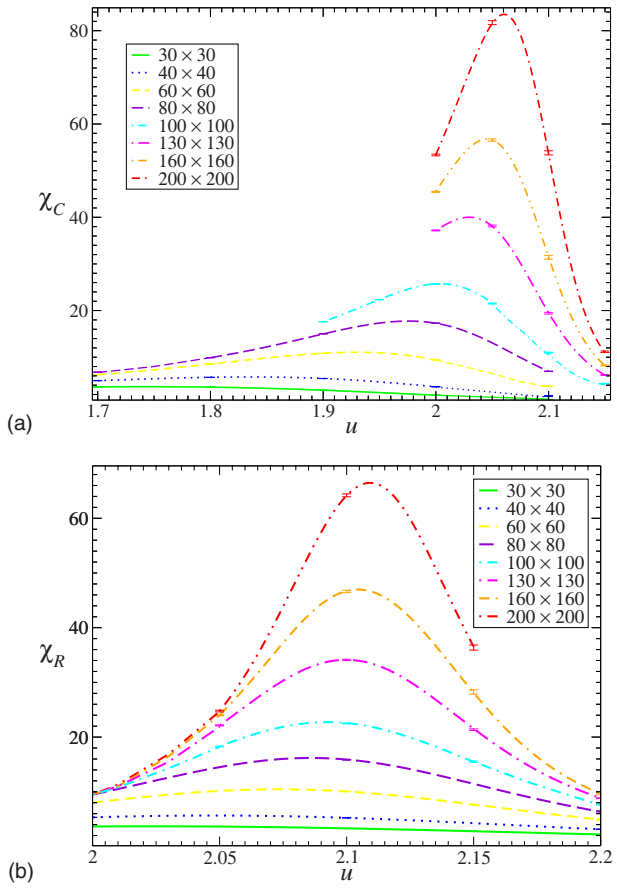

FIG. 6. (Color online) Classical susceptibilities of (a) the columnar order parameter C and (b) the orientational order parameter R for ρ_h=0.06. The magnitude and position of the maxima for different lattice sizes L can be used to extract the critical exponents γ and ν.

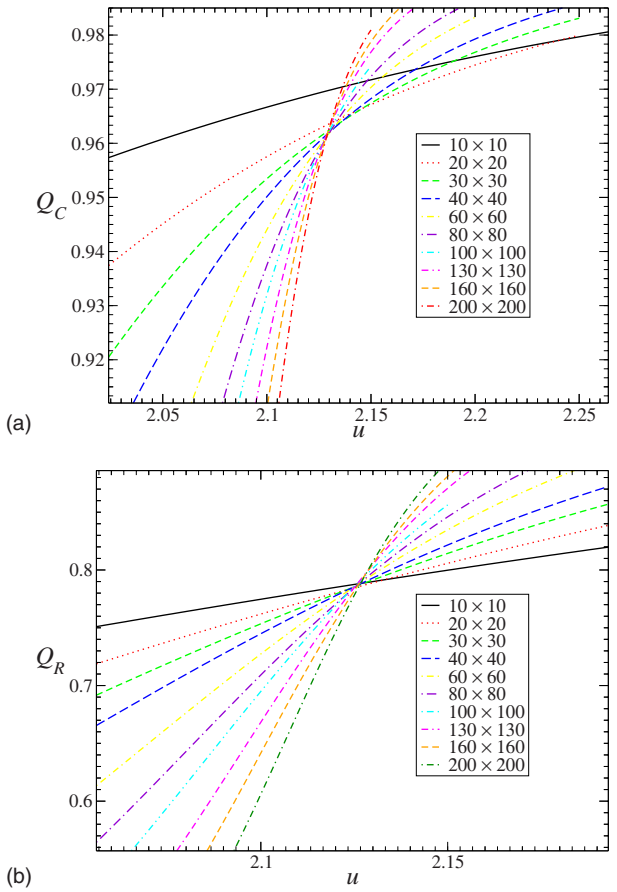

FIG. 7. (Color online) Fourth-order amplitude ratios of (a) the columnar order parameter C and (b) the orientational order parameter R for ρ_h=0.06. The clear crossings of the curves for different system sizes indicate a regular continuous phase transition.

change continuously along the phase boundary.

To test this prediction, we extract the anomalous dimensions η_C and η_R (which are equal to twice their scaling dimension) by means of finite-size scaling. The maximum of the susceptibility scales as $\chi^{\max} \sim L^{2-\eta} + \cdots$. Subleading scaling contributions are omitted in the fitting expression since the results for sufficiently large lattice sizes satisfy simple scaling (cf. Figs. 8 and 9).

The correlation-length exponent ν can be extracted from the slope of the fourth-order amplitude ratios of both order parameters at the critical point. Here, instead, we obtain it from the scaling behavior of the location of susceptibility maximum, which scales as $u_{\chi^{\max}} = u_c + \text{const} \times L^{-1/\nu} + \cdots$ [cf. Figs. 8(b) and 9(b)]. The critical coupling u_c, in turn, is obtained from the crossing points of the fourth-order amplitude ratio (Fig. 7).

By repeating this procedure for different hole densities, we find η_C and η_R, as well as ν as a function of ρ_h. We note that for the *undoped* case, the (logarithmic) finite-size corrections are so strong that the anomalous exponents are very difficult to determine. By including subleading corrections to the susceptibility expressions at the KT transition, we find strong indications that $\eta_C = 1/4$ and $\eta_R = 1$, satisfying the established theoretical description of this KT transition. The density dependence of the exponents is shown in Fig. 10(a). Clearly, they behave very differently: For the columnar parameter C, its anomalous dimension remains unchanged and equal to 1/4, while for R, it decreases monotonically from 1 to 1/4 where the transition is expected to become first order, according to the scenario presented in Sec. IV B. The results from our Monte Carlo simulations are thus consistent with the predictions we made in our theoretical analysis.

The evolution of the correlation-length exponent along the phase boundary is shown in Fig. 10(b). This exponent behaves *qualitatively* as predicted for finite doping, i.e., it exhibits a monotonically decreasing behavior along the line of fixed points. A direct *quantitative* comparison to the field-theoretical prediction is not possible, since the simulations are performed in the canonical ensemble. Even though the dimer density could be mapped to a *dimer* fugacity, the field theory assumes a fixed-hole fugacity. In addition, the evolution of the exponent in Fig. 10(b) is slower than predicted because in the simulations, we do not approach the phase boundary perpendicularly in the simulations, which leads to an *effective* exponent ν that is smaller than the one computed from the scaling dimension of the relevant operator in the field theory.

In Fig. 11, we summarize our results for the location of the phase boundary between the dimer-hole liquid phase and

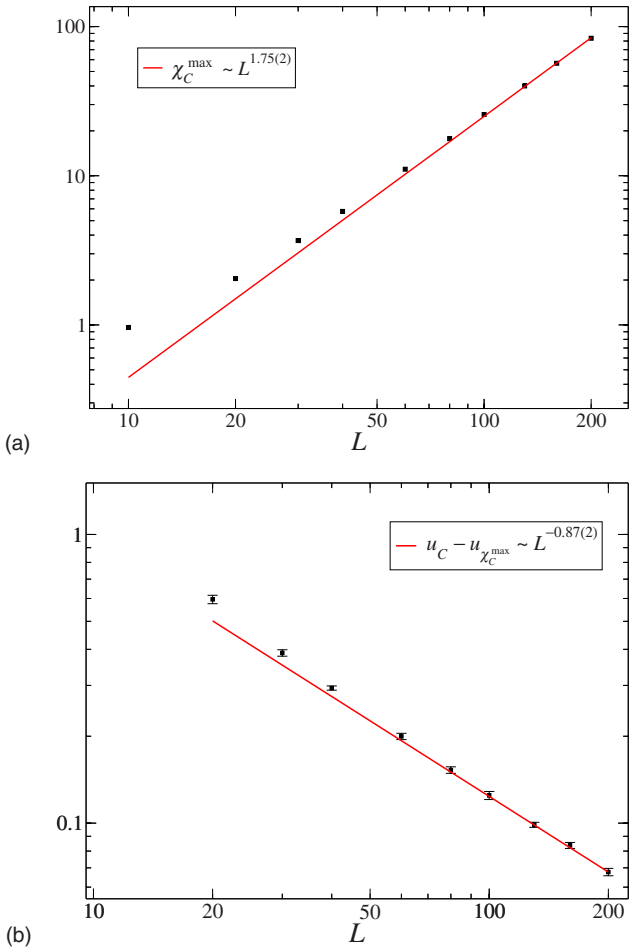

FIG. 8. (Color online) Finite-size scaling analysis of the susceptibility of the columnar order parameter C for $\rho_h=0.06$. (a) Scaling of the height of the maximum as a function of system size L. (b) Scaling of the position of the maximum. The critical value u_c is obtained from the crossing of the fourth-order cumulants (cf. Fig. 7). The same power-law behavior of the susceptibility maximum is found for all hole densities $\rho_h \leqslant 0.06$.

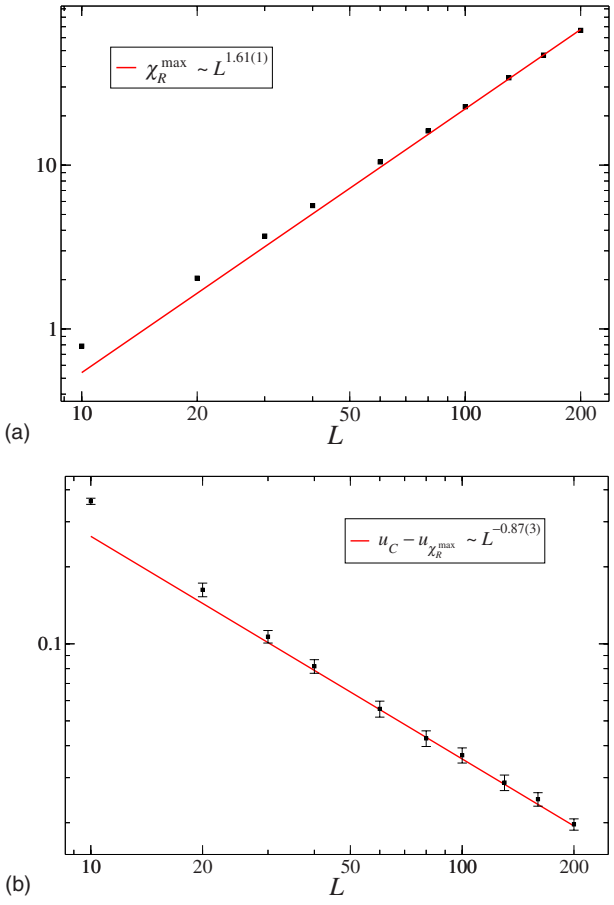

FIG. 9. (Color online) Finite-size scaling analysis of the susceptibility of the orientational order parameter R for $\rho_h=0.06$. (a) Scaling of the height of the maximum as a function of system size L. (b) Scaling of the position of the maximum. The critical value u_c is obtained from the crossing of the fourth-order cumulants (cf. Fig. 7). Unlike the results for the columnar order parameter (Fig. 8), the power-law behavior of the susceptibility maximum is now dependent on the hole density, consistent with an anomalous scaling exponent that varies along the phase boundary.

the columnar solid phase for hole densities $\rho_h \leqslant 0.06$. The behavior of the critical line for $\rho_h \to 0$ is consistent with its expected scaling behavior $\rho_h \propto \xi^{-2}(\rho_h=0)$, which is based on simple dimensional analysis, with the only length scale of the problem being the correlation length of the undoped problem.

D. High doping: First-order transition and phase separation

Beyond the multicritical point predicted in Secs. III and IV B (see also Appendix A), we expect a first-order transition line in the $z_{d\text{-}u}$ phase diagram, where z_d denotes the dimer fugacity. This line separates the crystalline from the liquid phase. According to our scenario, an entropic attraction between holes on the same sublattice becomes marginal and leads naturally to phase separation between a hole-rich liquid phase and a hole-poor columnar crystalline phase. Since the multicritical point is characterized by a marginally relevant operator, complicated crossover will be observed in the first-order transition region in the vicinity of this point.[66]

In addition, close to the multicritical point, the first-order transition will be very weak, with a discontinuity that vanishes with an essential singularity as a function of the distance to the multicritical point along the phase coexistence curve. At this transition, all observables, such as the latent heat, should vanish in a similar way, making the numerical study of the transition close to the multicritical point particularly difficult.

To confirm the existence of the discontinuous transition, we perform grand-canonical Monte Carlo simulations with single-dimer insertions and deletions (alternated with canonical geometrical cluster moves to accelerate the relaxation of the configurations), for couplings $u=3.0, 3.5, 4.0, 5.0, 6.0$, as a function of the dimer fugacity z_d. Figure 12(a) shows the dimer density as a function of dimer chemical potential μ_d. Although with increasing system size a jump in the dimer density develops, it does not become very pronounced. However, consideration of the heat capacity C_V [Fig. 12(b)] confirms the presence of a single phase transition at fixed coupling constant u, as C_V exhibits a peak at a chemical

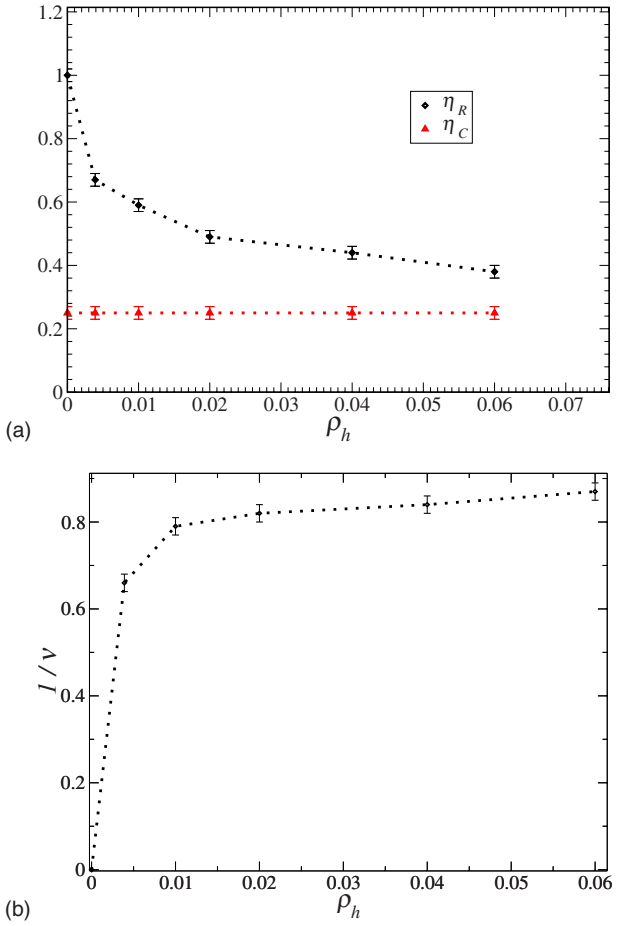

FIG. 10. (Color online) (a) Evolution of the anomalous dimensions η_C (lower curve) and η_R (upper curve) for the columnar and orientational order parameters, respectively, along the critical line for hole densities $0.004 \leqslant \rho_h \leqslant 0.06$. The transition will become first-order when the two curves cross. (b) The inverse correlation-length exponent $1/\nu$ as a function of doping along the critical line for hole densities $0.004 \leqslant \rho_h \leqslant 0.06$. Up to small systematic deviations discussed in the text, the observed trend agrees with the scaling predictions.

potential that matches the location of the jump in ρ_d. We emphasize that this classical heat capacity is not the heat capacity of the (2+1)-dimensional QDM. Indeed, C_V does not have any physical meaning in terms of the ground-state wave function that we are considering, because the ground-state energy cannot be changed through variation of the parameters u or μ_d. Another confirmation of the phase transition is obtained from the susceptibilities of the orientational [Fig. 13(a)] and columnar [Fig. 14(a)] order parameters, χ_R and χ_C, respectively. Both quantities exhibit a peak at a chemical potential that approaches, with increasing system size, the location of the peak observed in C_V.

To confirm the nature of the phase transition, we consider the scaling of the peaks in C_V, χ_R, and χ_C. For a first-order transition, these quantities should exhibit a δ-function singularity in the thermodynamic limit, or, equivalently, for finite systems, their peaks must scale with the lattice size in a finite system. We find that the heat-capacity peak, apart from a constant background, indeed scales with the lattice size L^2

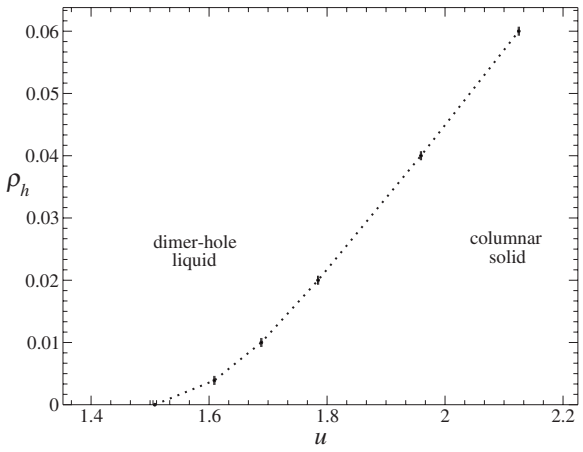

FIG. 11. Phase diagram at low doping, with the critical line of fixed points separating the dimer-hole liquid phase $[u < u_c(x)]$ from the columnar solid $[u > u_c(x)]$.

for the range of system sizes (up to $L=140$) that we considered. This is supported by the behavior of the system-size dependent maxima in χ_R and χ_C, see Figs. 13 and 14, which both scale as L^2, indicating that $\eta=0$. In addition, all local order parameters must develop a discontinuity at the transition point as the system size increases. Whereas the jump in the dimer density [Fig. 12(a)] is not very sharp, the jump in the columnar and orientational order parameters, C and R, is quite pronounced already for the system sizes studied here, see Figs. 15(a) and 15(b). Furthermore, the location the order parameter jump provides a good indication of the transition point.

The strongest evidence, however, is provided by the fourth-order amplitude ratio of the density, Q_ρ. At a first-order transition, this quantity displays a specific behavior, as discussed in Ref. 70. In particular, the positions of two minima observed in Fig. 16(a) approach, in the thermodynamic limit, the densities of the two coexisting phases. Outside the coexistence region, Q_ρ approaches a limiting value of 1/3, characteristic of Gaussian fluctuations. This type of behavior is not found at a continuous phase transition and should be considered as a strong indicator for the occurrence of a first-order transition. This is particularly important since the very weak nature of the first-order transition makes it impossible to unambiguously confirm the existence of a double peak in the histograms of the internal energy for the system sizes that we considered. Whereas the first-order transition becomes more pronounced at higher couplings, and it thus should become easier to distinguish the two peaks in the energy histogram, in practice, those simulations are seriously hampered by the very large relaxation times encountered for large dimer interactions.

By repeating the analysis presented here for different couplings, and estimating the coexistence chemical potential from the convergence point observed at the order-parameter discontinuity (cf. Fig. 15), we derive the phase diagram in the z_d-u plane, see Fig. 16(b).

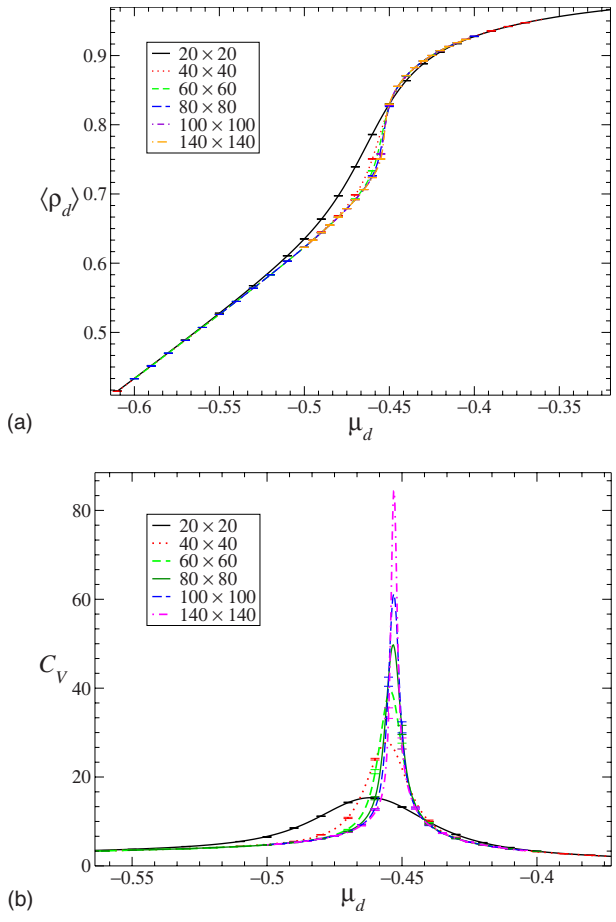

FIG. 12. (Color online) (a) The ρ_d-μ_d equation of state for coupling $u=3.5$ and different lattice sizes. As the system size increases, the jump in the dimer density at the first-order phase transition gradually becomes more pronounced but remains relatively weak. (b) The heat capacity of the classical interacting dimer model for the same coupling strength. We find that the peak scales as $C_{\max} \sim C_0 + L^2$, providing strong evidence for a first-order transition at $u=3.5$.

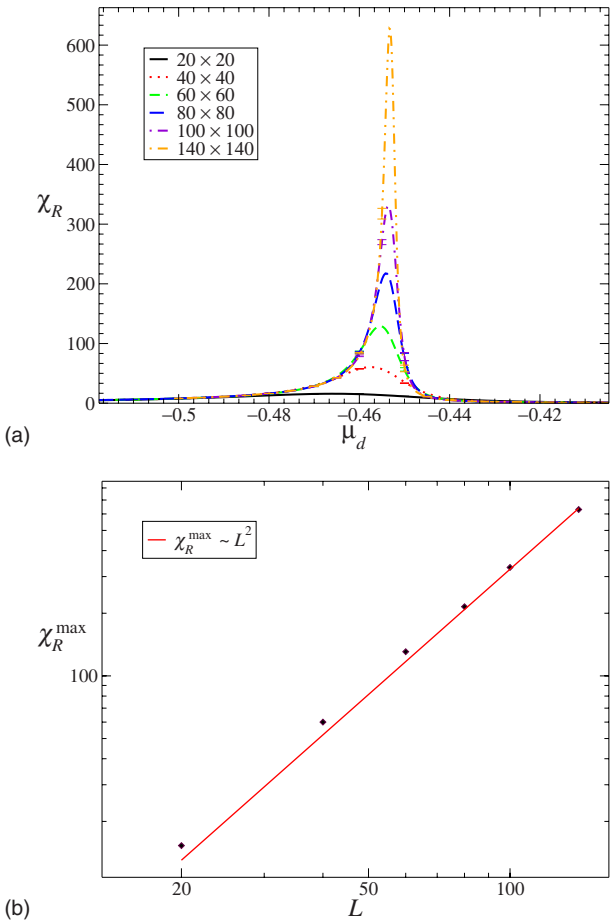

FIG. 13. (Color online) (a) Susceptibility of the orientational order parameter R for coupling $u=3.5$ and different lattice sizes. (b) Asymptotically, the maxima of χ_R scale with the lattice size, confirming the first-order nature of the phase transition.

VI. EFFECTS OF REPULSIVE HOLE-HOLE INTERACTIONS NEAR THE FIRST-ORDER TRANSITION REGION

We now discuss briefly the effects of additional interactions near the coexistence curve. It is clear that additional interactions near the first-order transition line should stabilize more complex ordered inhomogeneous phases. The simplest interaction that competes with the tendency of holes to pair and phase separate from the crystal is a weak nearest-neighbor hole-hole repulsion V_h. The addition of such an interaction to the classical dimer model would lead to an additional energy cost for homogeneous and isotropic clusters of holes. Remarkably, for a range of dimer interactions u, this energy cost leads to the formation of commensurate hole stripes with period of 3, in a region in the phase diagram located between the dimer-columnar crystal and the hole-dimer liquid. For general values of u, V_h, and hole densities, one expects a complex phase diagram, most likely similar to what is found in theories of commensurate-incommensurate transitions, which we do not explore here in detail but are discussed in Refs. 71–74.

This phase can be thought of as the ground-state wave function of a quantum Hamiltonian constructed using the approach described in Sec. II. The quantum Hamiltonian that leads to the prescribed wave function includes a generalized form of the hole-related Hamiltonian of Eq. (2.6),

$$H = H_d + t_{\text{hole}} \sum_i [-|C_i^h\rangle\langle C_i^{h'}| - |C_i^{h'}\rangle\langle C_i^h| + y^{R_{C_i^{h'}} - R_{C_i^h}} |C_i^h\rangle\langle C_i^h| + y^{R_{C_i^h} - R_{C_i^{h'}}} |C_i^{h'}\rangle\langle C_i^{h'}|], \tag{6.1}$$

where $R_{C_i^h}$ and $R_{C_i^{h'}}$ denote the number of pairs of holes formed in the corresponding configurations C_i^h and $C_i^{h'}$ (cf. Fig. 17). More specifically, the ground-state wave function is

$$|G_{N_h}^{int}\rangle = \frac{1}{\sqrt{Z(w^2, y^2, N_h)}} \sum_{\{\mathcal{C}_{N_h}\}} w^{N_p^d[\mathcal{C}_{N_h}]} y^{N_p^h[\mathcal{C}_{N_h}]} |\mathcal{C}_{N_h}\rangle. \tag{6.2}$$

This wave function has a counterpart in the grand-canonical ensemble, for which the exactly solvable quantum Hamiltonian is a generalization, in exactly the same way as above, of Eq. (2.8).

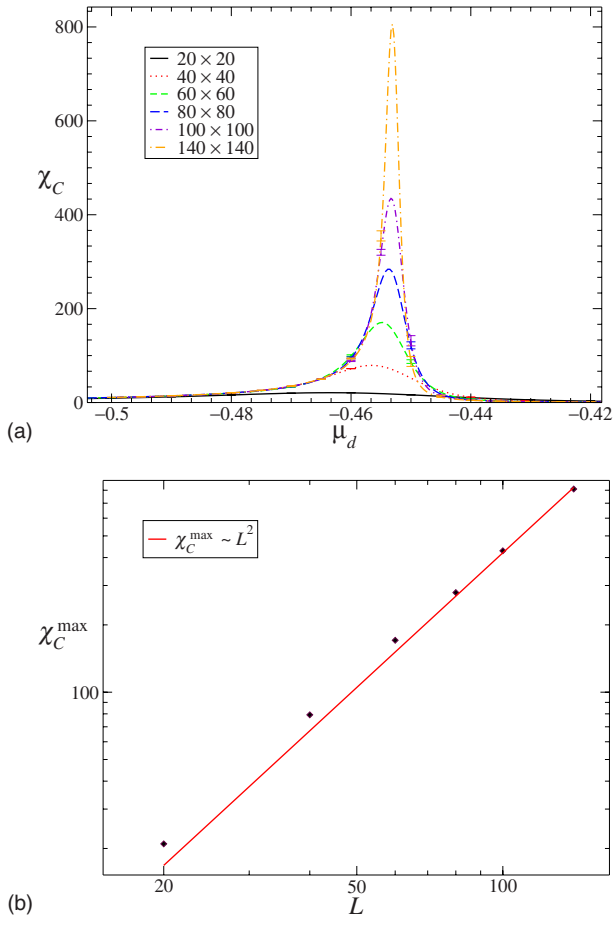

FIG. 14. (Color online) (a) Susceptibility of the columnar order parameter C for coupling $u=3.5$. (b) The maxima of χ_C as a function of the linear lattice dimension. As for χ_R [Fig. 13(b)], the maxima scale with lattice size, supporting the occurrence of a δ-function singularity in χ_C in the thermodynamic limit, as expected for a first-order phase transition.

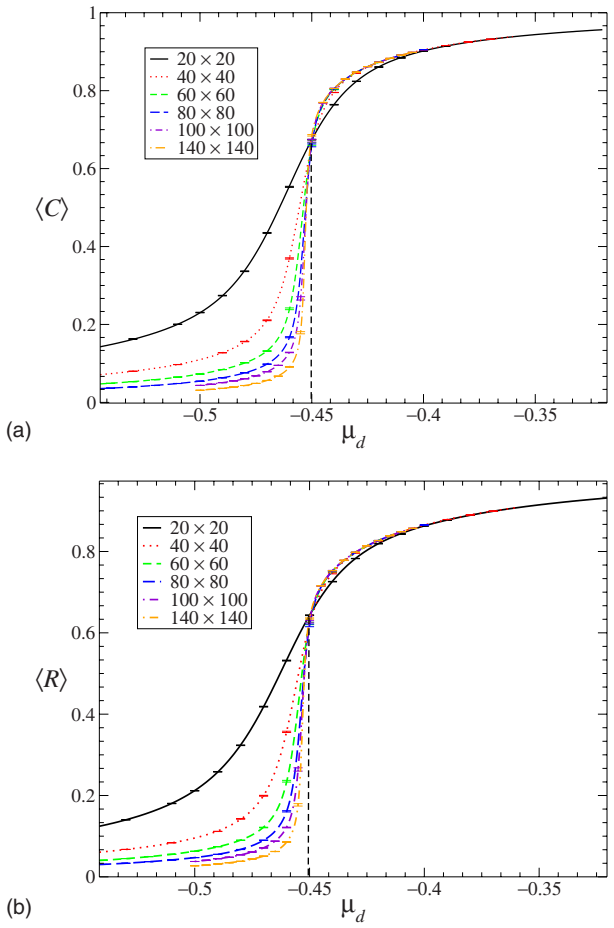

FIG. 15. (Color online) (a) The columnar order parameter C as a function of the dimer chemical potential μ_d for coupling $u=3.5$. The rapid increase near the transition becomes more pronounced as the thermodynamic limit is approached. The dashed line shows the approximate position of the transition point. (b) The orientational order parameter R as a function of the chemical potential μ_d for coupling $u=3.5$. It also shows a rapid increase similar to the behavior of C, at the same chemical potential.

By performing grand-canonical simulations for weak hole repulsions, $V_h \leq \frac{1}{10}u$, in the regime of strong dimer attractions, $u>4.0$, where the first-order transition is more pronounced, a hole-stripe phase was observed. In particular, for the couplings $u=5.0$, $V_h=0.5$, and a dimer chemical potential $-1.1<\mu_d<-0.8$ (i.e., between the liquid phase $\mu_d \lesssim -1.2$ and the columnar phase $\mu_d \gtrsim -0.8$), the hole density structure factor shows nontrivial peaks at $(k_x,k_y)=(\pm 2\pi/3,0)$, $(0,\pm 2\pi/3)$, which sharpen as the lattice size increases (see Fig. 18). A snapshot of the ordered phase (Fig. 19) illustrates how the holes order in stripes with a period of three lattice spacings, whereas the dimers are still ordered in a columnar pattern. In this way, the holes minimize the effect of the hole-hole repulsions and the dimers simultaneously maximize the effect of the attractive dimer-dimer interactions. The same pattern is also found for $u=4.0, 4.5, 6.0$, in similar regimes for the hole-hole interaction.

More generally, we expect that, as the liquid phase is approached in the regime of strong dimer couplings, a sequence of hole-commensurate phases will be stabilized, leading ultimately to incommensurate phases next to the liquid phase. The formation of this phase diagram is similar in spirit to the ones discussed in Refs. 71–74.

VII. ELEMENTARY QUANTUM EXCITATIONS OF DOPED QUANTUM DIMER MODELS

In the preceding two sections, we discussed the properties of the ground-state wave functions and the behavior of equal-time correlation functions of several operators of physical interest. There we used extensively the connection that exists for these types of wave functions between the computation of equal-time correlators of local operators and computations of similar objects in the equivalent two-dimensional classical statistical mechanical system of interacting dimers and holes. In this section, we will be interested in the spectrum of low-lying excitations, which is inherently a quantum-mechanical property.

Unfortunately, as it usually the case in QDMs,[1] all we know is the ground-state wave function. The low-lying excitation spectrum is not known exactly but it can be computed approximately using the variational principle. This is the single-mode approximation (SMA), which is a useful tool for studying the excited states of many-body systems.[75–79] It is

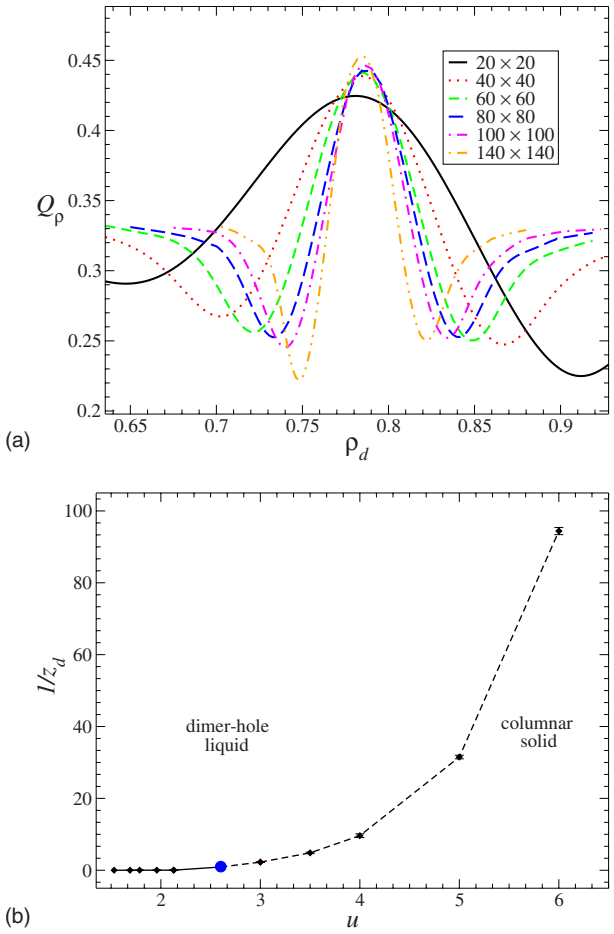

FIG. 16. (Color online) (a) Fourth-order amplitude ratio for the dimer density at coupling $u=3.5$. The exhibited behavior is typical of a first-order transition (Ref. 70), with two minima in the thermodynamic limit approaching the coexisting densities. (b) Phase boundary between the dimer liquid and the columnar solid. For low couplings, the transition is continuous (solid line). Our best estimate for the multicritical point ($u_c \approx 2.6$) is represented by the large circular dot. Beyond the multicritical point, the phase boundary (dashed line) is estimated from grand-canonical MC simulations at fixed *dimer fugacity* z_d.

particularly useful in the case of quantum dimer models at their RK points due to the fact that the exact ground-state wave function is known exactly. The computation of the low-

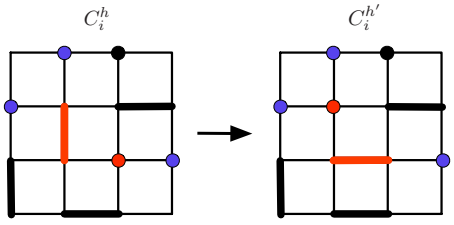

FIG. 17. (Color online) A particular hopping process realized in the Hamiltonian [Eq. (6.1)]. The potential terms that are present in the Hamiltonian depend on the number of additional pairs of holes that are formed after the hopping process. In the process shown above, this number is 1.

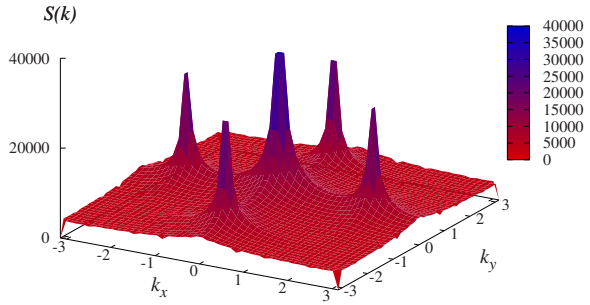

FIG. 18. (Color online) The hole density structure factor $S(k)$ for dimer coupling $u=5.0$, hole repulsion $V_h=0.5$, and dimer chemical potential $\mu_d=-1.0$, for linear system size $L=128$. The four peaks at $(\pm 2\pi/3, 0)$ and $(0, \pm 2\pi/3)$ correspond to the ordered configuration of hole stripes shown in Fig. 19.

lying collective modes in the QDM was done by Rokhsar and Kivelson.[1] Alternatively, one can describe qualitatively the low-lying spectrum using the effective field theory of the quantum dimer models (and their generalizations) at criticality, the *quantum Lifshitz model* of Ref. 11.

In this section, we will consider only the SMA spectrum in the dimer-hole liquid phase. Similar calculations can be done in the phase with long-range columnar order. In the dimer-hole liquid phase, the equal-time correlation function of the hole density operator, i.e., the one-body density matrix, approaches a constant at long distances. Thus, the wave function for this phase exhibits a Bose condensate of holes. Since the holes are charged, this is a charge Bose condensate. To determine if it is a superfluid (or more precisely a superconductor), it is necessary to show that it has a finite superfluid stiffness, i.e., a critical velocity. This can be determined form the spectrum of density fluctuations and hence from the spectrum of collective modes. It will turn out that, in spite of the more correlated nature of the wave functions we consider here, the result will be similar to that of Rokhsar and

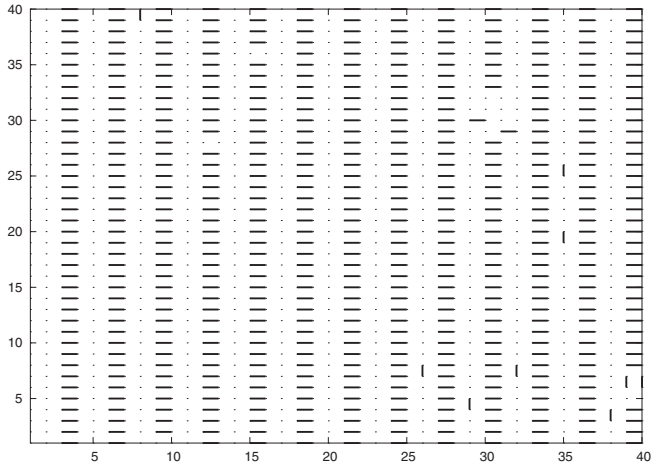

FIG. 19. Snapshot of a part of a typical ordered configuration that appears at the couplings $u=5.0$, $V_h=0.5$, $\mu_d=-1.0$, and linear system size $L=128$. Holes prefer to form commensurate stripes of period of 3, so as to minimize the effect of the weak hole repulsions.

Kivelson,[1] i.e., no superfluid stiffness. Given the more general structure (while still local) of the wave functions we study here, we conclude that wave functions associated with Hamiltonians satisfying the RK condition, in general, do not describe superfluid states.

We begin by summarizing the SMA procedure, focusing on doped quantum dimer models. Firstly, one must know the exact ground state of the system $|0\rangle$ and the type of excitations which saturate the frequency sum rule. In our case, there are two candidates: the dimer density and the hole density excitations. Since it follows from a variational principle, the SMA provides a proof of existence only for gapless excitations but not for gapped ones. The energy of an excitation created by an operator with wave vector $\mathbf{k}$, which we will denote by $\hat{\rho}_{\mathbf{k}}$, acting on the ground state is bounded from above as follows:[75–77]

$$E_{\mathbf{k}} - E_0 \leqslant \frac{f(\mathbf{k})}{s(\mathbf{k})} = \frac{\langle 0|[\hat{\rho}(-\mathbf{k}),[\mathcal{H},\hat{\rho}(\mathbf{k})]]|0\rangle}{\langle 0|\hat{\rho}(-\mathbf{k})\hat{\rho}(\mathbf{k})|\mathbf{0}\rangle}, \tag{7.1}$$

where $f(\mathbf{k})$ is the "oscillator strength" and $s(\mathbf{k})$ is the structure factor (i.e., the equal-time correlation function) for the operator $\hat{\rho}(\mathbf{k})$.

In the case of doped QDMs at their RK point, we know their ground-state wave functions exactly and they have (by construction) zero ground-state energy, $E_0=0$. Thus, the excitation spectrum must be positive. The system will have gapless excitations if $E_{\mathbf{k}}-E_0$ vanishes at some wave vector. It is worth noting that there are two distinct ways for the SMA bound to vanish close to some $\mathbf{k}=\mathbf{k}_0$. One way is if $f(\mathbf{k})$ vanishes at $\mathbf{k}_0$. This can happen only if the commutator $[\mathcal{H},\hat{\rho}(\mathbf{k}_0)]$ vanishes. This means that $\rho(\mathbf{k}_0)$ is a conserved quantity. The other way occurs when $s(\mathbf{k})$ becomes infinite at $\mathbf{k}_0$. This is a signature of a nearby density-ordered state like the columnar dimer crystal we found in the phase diagram of the dimer models under study, shown in Fig. 2.

In the following, we will use the following operator definitions. For dimers, $\hat{\sigma}^d_{\hat{\alpha}}(\mathbf{r})$ denotes the dimer-density operator and it takes the values of ± 1 if a dimer is present or absent at the link which begins at the position $\mathbf{r}$ and has direction $\hat{\alpha}=\hat{x},\hat{y}$. For holes, $\hat{\sigma}^h(\mathbf{r})$ denotes the hole density operator and it takes the values of ± 1 if a hole is present or absent at the position $\mathbf{r}$.

Details of the derivations of the SMA oscillator strength functions for both models are given in Appendix B. Here, we just quote the main results.

A. Fixed-hole-density model

1. Hole density excitations

For the fixed-hole-density model, the SMA oscillator strength function $f(\mathbf{k})$ for hole density excitations is given by

$$f(\mathbf{k}) = 4t_{\text{hole}}\mathbf{q}^2 \tag{7.2}$$

for $\mathbf{k}=(\pi,\pi)+\mathbf{q}$.

From the results of the Sec. III and Appendix A, we may conclude that for $\mathbf{k}=(\pi,\pi)+\mathbf{q}$, the structure factor near (π,π) scales like $s^{(\pi,\pi)}(\mathbf{k}) \propto \frac{1}{q^2+\xi^{-2}}$ and, thus, $s^{(\pi,\pi)}(0)$ is a constant. Thus, $E^{(\pi,\pi)}_{\mathbf{k}} - E_0 \propto \mathbf{q}^2$. For $\mathbf{k}=(0,0)+\mathbf{q}$, the results from the following section, which formally hold only for low density of dimers, lead to the conclusion that $s^{(0,0)}(\mathbf{k}) \propto \frac{1}{q^2-\xi^{-2}}$ and $s^{(0,0)}(0)$ is again a constant but has strong oscillatory behavior in real space. Thus, from the correlation function we computed in Appendix A, we conclude that these excitations are also quadratic in the momentum $\mathbf{q}$, i.e., $E_{\mathbf{k}}-E_0 \leqslant \mathbf{q}^2$. This result is consistent with the compressibility argument, given in Ref. 1, which would also give quadratic dispersion in this case [keeping in mind that in this case, the compressibility is infinite when the system is doped (constant number of holes)]. However, it is important to stress that the compressibility argument is a stronger condition because our calculation of the correlation function is legitimate for low dimer densities.

2. Dimer-density excitations

For the fixed-hole-density model, the SMA oscillator strength function $f(\mathbf{k})$ for dimer-density excitations is given by

$$f(\mathbf{k}) = f_{\text{dimer-flip}}(\mathbf{k}) + f_{\text{hole(1)}}(\mathbf{k}) \tag{7.3}$$

Close to the wave vector $\mathbf{Q}_0=(\pi,\pi)$ with $\mathbf{k}=\mathbf{Q}_0+\mathbf{q}$, both oscillator strengths $f_{\text{dimer-flip}}(\mathbf{k})$ and $f_{\text{hole(1)}}(\mathbf{k})$ vanish quadratically (cf. Appendix B) and more specifically,

$$f_{\text{dimer-flip}}(\mathbf{q}) = 8tq^2, \tag{7.4}$$

$$f_{\text{hole(1)}}(\mathbf{q}) = -t_{\text{hole}}q^2. \tag{7.5}$$

Given the fact that the dimer-density structure factor is a constant at $Q_0=(\pi,\pi)$ and combining Eqs. (B12) and (7.3) we may conclude that there are gapless dimer-density excitations at $Q_0=(\pi,\pi)$.

In addition to these results, we may have additional branches of dimer-density excitations, especially when there is a divergence of the structure factor at some wave vector $\mathbf{Q}_0$ which would be an indication of dimer order at a nearby phase. In particular, this happens at the phase boundary between the hole-dimer liquid phase and the columnar-ordered crystalline phase.

B. Fixed-hole fugacity model

As above, we can study the hole density excitations of the second model, the grand-canonical model, in which the hole density is not fixed but is determined by a parameter z which plays the role of a hole fugacity in the wave function. By the fact that there is no conservation of the number of holes is explicitly broken, we can predict that the numerator $f(\mathbf{k})$ will vanish only at $\mathbf{Q}_0=(\pi,\pi)$. This happens because of the bipartite lattice symmetry that enforces the number holes on each sublattice to be equal. For the fixed-hole fugacity model, the SMA oscillator strength function $f(\mathbf{k})$ for hole density excitations is

$$f_{\text{hole(2)}}(\mathbf{k}) = 4t_{\text{pairing}}[2+\cos(\mathbf{k}_x)+\cos(\mathbf{k}_y)]. \tag{7.6}$$

The formula shows that the numerator $f_{\text{hole(2)}}(\mathbf{k})$ vanishes only at the wave vector $\mathbf{Q}_0=(\pi,\pi)$ quadratically, as ex-

pected. The dimer-density excitations are not gapless (in the sense that the numerator does not vanish for any $\mathbf{Q}_0$), because the dimer-flip contribution vanishes at $(\pi,\pi),(0,\pi)$ and the dimer-breaking term gives a constant contribution. This is expected due to the violation of the dimer number conservation. It is important to stress that the behavior of the structure factor is exactly the same as before (in the fixed-hole-density model). The reason is the equivalence of the canonical and grand-canonical ensembles in the thermodynamic limit for classical systems.

It is certainly worth noting that, although the two ground-state wave functions of Eqs. (2.7) and (2.9) have the same ground-state physics, due to the essential equivalence of the classical canonical and grand-canonical ensembles in the thermodynamic limit, the nature of their quantum elementary excitations is drastically different.

VIII. CONCLUSIONS

In this work, we have constructed generalizations of the quantum dimer model to include the effects of dimer correlations as well as finite hole doping in the wave function. Throughout, we considered the case of bosonic (charged) holes and neglected the fermionic spinons. We have constructed generalized RK Hamiltonians whose ground-state wave functions describe the effects of (attractive) dimer correlations and finite hole doping. We have discussed the rich phase diagram and critical behavior of three doped interacting quantum dimer models at their RK point using both analytic methods and numerical simulations. We have shown that the ground-state wave function embodies a complex phase diagram which consists of dimer-hole liquid and columnar phases separated by a critical line with varying exponents, ending at a multicritical point with a Kosterlitz-Thouless structure where the transition becomes first order. The critical behavior along the low-doping section of the phase boundary was investigated in detail, and the predictions of our scaling analysis were confirmed with large-scale Monte Carlo simulations. Monte Carlo simulations were also used to show that the transition between the dimer-hole liquid and the columnar solid does indeed become first order and to estimate the location of the multicritical point and of the first-order phase boundary.

In the high-doping regime, near the first-order transition line, additional repulsive interactions among holes were shown to generate, at the expense of the two-phase region, an even richer phase diagram with phases in which the dimer-hole system becomes inhomogeneous. In the regime of strong dimer coupling, $u=5=0$, and weak hole interactions, $V_h=0.5$, we found a stripe phase with wave vectors $(2\pi/3,0)$ and $(0,2\pi/3)$. In general, we expect the two-phase region to be replaced by a complex phase diagram with a large number of commensurate and incommensurate phases. This physics is well known in the context of two-dimensional classical statistical mechanics of systems with competing interactions.[71–73] However, it is interesting to see how it arises at the level of the exact ground-state wave function of models of strongly correlated systems, particularly given the current interest on this type of phenomena in high-temperature superconductors and related systems.[13,80–84]

In this paper, we have also presented an analysis of the low-lying excitations of the quantum system and found that, much as in the case of the Rokhsar-Kivelson quantum dimer model, the doped system is a Bose-Einstein condensate but not a superfluid, since the superfluid stiffness vanishes even though both dimers and holes interact. It is apparent that in order to render the Bose-Einstein condensate a true superfluid, it is necessary to violate the RK condition which forces the wave function to have a local structure. The effects of violations to the RK condition are poorly understood, and we have not investigated this important problem which is essential in determining the generic phase diagram of these models.

ACKNOWLEDGMENTS

We thank C. Castelnovo, C. Chamon, P. Fendley, S. Kivelson, M. Lawler, R. Moessner, C. Mudry, V. Pasquier, P. Pujol, K. S. Raman, S. Sondhi, and M. Troyer for many discussions. This work was supported in part by the National Science Foundation through Grant No. NSF DMR 0442537 (E.F.) and CAREER Award No. NSF DMR 0346914 (E.L.) and by the U.S. Department of Energy, Division of Materials Sciences under Award No. DEFG02-91ER45439, through the Frederick Seitz Materials Research Laboratory at the University of Illinois at Urbana-Champaign (E.L. and E.F.). The calculations presented here were in part performed at the Materials Computation Center of the Frederick Seitz Materials Research Laboratory at the University of Illinois at Urbana-Champaign (E.L.), at the Turing XServe Cluster at the University of Illinois, and at NCSA Teragrid cluster facilities under Award No. PHY060022.

APPENDIX A: MEAN-FIELD THEORY FOR DIMERS AND HOLES

In this appendix, we give details of the mean-field theory summarized in Sec. III. We will use Grassmann variable methods to write down the partition functions for classical interacting and doped dimers. We will use these methods to derive a simple mean-field theory for this system. While mean-field theory, as it is well known, fails to give the correct critical behavior in two-dimensional systems, it offers a good qualitative description of the phases and, surprisingly, even of the gross features of the phase diagram. In subsequent sections, we will use more sophisticated analytic and numerical methods to study the phase transitions.

1. Noninteracting dimers at finite hole density

The classical dimer-hole partition function can be formulated in terms of a Grassmann functional integral, according to the prescription of Ref. 32. The classical partition function of the dimer problem on any lattice, which is defined by the connectivity matrix M and with fugacity z for the dimers and 1 for the holes, is

$$\mathcal{Z}_{\text{dimer}} = \int \mathcal{D}\eta\mathcal{D}\eta^{\dagger} \exp\left(\sum_i \eta_i\eta_i^{\dagger} + \frac{z}{2}\sum_{ij} M_{ij}\eta_i\eta_i^{\dagger}\eta_j\eta_j^{\dagger}\right). \tag{A1}$$

For the square lattice, M_{ij} is 1 if i,j are nearest-neighbor sites and zero otherwise. For the triangular lattice, M_{ij} is 1 if i,j are nearest neighbors and also next-nearest-neighbor sites, but only along one diagonal, i.e., if $j=i+\hat{\mathbf{x}}+\hat{\mathbf{y}}$ or $j=i-\hat{\mathbf{x}}-\hat{\mathbf{y}}$. Also, the fugacity z ranges from 0 to ∞. When $z\to 0$, the system is filled with holes and there are very few dimers, and when $z\to\infty$, the system approaches the close-packed limit with dimers. Both limits are worth of study due to the existence of an important theorem by Heilmann and Lieb,[85] which proves under rather general assumptions the absence of any phase transitions with doping in this model. Thus, the identification of the phase in the *few dimer* limit is enough to conclude about the phase that the system enters when doped. In this section, we will study this problem in the limit in which the dimers are dilute. In this regime a simple mean-field theory of the Hartree type is expected to be accurate.[32] Such a crude approximation should break near criticality, i.e., near the close packing limit.

To proceed, we apply a Hubbard-Stratonovich transformation to the above partition function:

$$\exp\left(\frac{z}{2}\sum_{ij} M_{ij}\eta_i\eta_i^{\dagger}\eta_j\eta_j^{\dagger}\right) = \mathcal{N}\int \mathcal{D}\phi \exp\left(-\frac{1}{2z}\sum_{ij}\phi_i M_{ij}^{-1}\phi_j + \sum_i \eta_i\eta_i^{\dagger}\phi_i\right), \tag{A2}$$

where $\mathcal{N}$ is an irrelevant normalization constant. We may also add sources for the hole density operators $J\eta\eta^{\dagger}$. In this way, the classical dimer partition function may be written as follows:

$$\mathcal{Z}_{\text{dimer}} = \int \mathcal{D}\phi\mathcal{D}\eta\mathcal{D}\eta^{\dagger} \exp\left(-\frac{1}{2z}\sum_{ij}\phi_i M_{ij}^{-1}\phi_j + \sum_i \eta_i\eta_i^{\dagger}(\phi_i + 1 + J_i)\right), \tag{A3}$$

where we have dropped the normalization constant $\mathcal{N}$, as we will do in what follows. (Note that what makes the above problem *unsolvable* is the term "1" in the exponent.)

Upon integrating out the Grassmann variables, we find

$$\mathcal{Z}_{\text{dimer}} = \int \mathcal{D}\phi \exp\left(-\frac{1}{2z}\sum_{ij}(\phi_i - J_i)M_{ij}^{-1}(\phi_j - J_j) + \sum_i \ln(\phi_i + 1)\right). \tag{A4}$$

In the limit $z\to 0$, we may formulate a legitimate and well-defined mean-field theory. To this end, we rewrite the partition function in the following way:

$$\mathcal{Z}_{\text{dimer}} = \int \mathcal{D}\phi \exp\left(-\frac{1}{z}\left[\frac{1}{2}\sum_{ij}(\phi_i - J_i)M_{ij}^{-1}(\phi_j - J_j) - z\sum_i \ln(\phi_i + 1)\right]\right) = \int \mathcal{D}\phi e^{-(1/z)\mathcal{S}(\phi)}, \tag{A5}$$

where

$$S(\phi) = \frac{1}{2}\sum_{ij}(\phi_i - J_i)M_{ij}^{-1}(\phi_j - J_j) - z\sum_i \ln(\phi_i + 1) \tag{A6}$$

is the effective action. As $z\to 0$, we have a theory which has a well-defined saddle point and the perturbation around this point will be in powers of z which plays the role of an effective coupling constant. In this way, we have a very fast convergent expansion.

The saddle-point is defined as follows:

$$\left.\frac{\delta\mathcal{S}}{\delta\phi_i}\right|_{\phi_i=\bar{\phi}} = 0, \tag{A7}$$

and we take the following equation for $\bar{\phi}$:

$$\bar{\phi}_i = J_i + z\sum_j \frac{M_{ij}}{\bar{\phi}_j + 1}. \tag{A8}$$

In this approximation, the density of holes is given by

$$\rho_i = \langle \eta_i\eta_i^{\dagger}\rangle = \frac{\partial \ln \mathcal{Z}_{dimer}}{\partial J_i} = -\frac{1}{z}\frac{\partial\mathcal{S}}{\partial J_i} = \frac{1}{\bar{\phi}_i + 1}. \tag{A9}$$

So, the source J_i in terms of the density of the holes ρ_i is given by

$$J_i = \bar{\phi}_i - z\sum_j \frac{M_{ij}}{\bar{\phi}_j + 1} = \frac{1}{\rho_i} - z\sum_j M_{ij}\rho_j - 1. \tag{A10}$$

The Legendre transform of the effective action $\mathcal{S}$ is

$$\Gamma(\rho_i) = \frac{1}{z}\mathcal{S}(\bar{\phi}_j(\rho_i), J_j(\rho_i)) + \sum_i J_i(\rho_j)\rho_i \tag{A11a}$$

$$= -\frac{z}{2}\sum_{ij}\rho_i M_{ij}\rho_j + \sum_i \ln(\rho_i) + \sum_i (1 - \rho_i). \tag{A11b}$$

We specialize now to the case of uniform hole density $\rho_i = \rho$ and also for the case of the square lattice where the number of nearest neighbors is $2D=4$ and assuming that the number of sites on the lattice is N. Then,

$$\Gamma(\rho) = -\frac{z}{2}(4N\rho^2) + N\ln(\rho) + N(1 - \rho). \tag{A12}$$

At this level of approximation ("Hartree"), the equation of state becomes

$$J = -4z\rho + \frac{1}{\rho} - 1. \tag{A13}$$

So, when the sources are set to zero, the density in terms of the fugacity, in the limit $z \to 0$, is

$$\rho = \frac{2}{1 + \sqrt{1 + 16z}}. \tag{A14}$$

As a check of the approximation, we may expand the result in the region of $z \to 0$, where the result should be $\rho \simeq 1$ for the hole density:

$$\rho = 1 - 4z + O(z^2). \tag{A15}$$

Or, equivalently, for $\rho \to 1^-$,

$$z = \frac{1}{4\rho}\left(\frac{1}{\rho} - 1\right) = \frac{1}{4}(1-\rho) + O((1-\rho)^2). \tag{A16}$$

The hole density-density correlation function can be obtained in the following way by using the Legendre transform:

$$\mathcal{G}_{ij} = \langle \eta_i \eta_i^\dagger \eta_j \eta_j^\dagger \rangle - \langle \eta_i \eta_i^\dagger \rangle \langle \eta_j \eta_j^\dagger \rangle = \frac{\partial^2 \ln Z_{dimer}}{\partial J_i \partial J_j} = \frac{\partial \rho_i}{\partial J_j}, \tag{A17}$$

and also

$$\mathcal{G}_{ij} = \left[\frac{\partial^2 \Gamma}{\partial \rho_i \partial \rho_j}\right]^{-1}. \tag{A18}$$

By using Eqs. (A11b) and (A18), we have

$$[\mathcal{G}_{ij}]^{-1} = \frac{\partial^2 \Gamma}{\partial \rho_i \partial \rho_j} = -zM_{ij} - \delta_{ij}\frac{1}{\rho_i^2}. \tag{A19}$$

Since M_{ij} is a function of the distance between sites and vanishes except for nearest neighbors, its Fourier transform is

$$M(\vec{q}) = a^2 \sum_i e^{-i\mathbf{q}\cdot(\mathbf{r}_i - \mathbf{r}_j)} M(\mathbf{r}_i - \mathbf{r}_j) = 2a^2 \sum_{\alpha=1}^{2} \cos q_\alpha a. \tag{A20}$$

Also, we set $a=1$, and finally, the hole density connected correlation function is

$$\mathcal{G}(\vec{q}) = \frac{1}{-\frac{1}{\rho^2} - 2z\sum_{\alpha=1}^{2} \cos q_\alpha}. \tag{A21}$$

For momenta near $\mathbf{Q}=(\pi,\pi)$, $\mathbf{q}=\mathbf{Q}+\mathbf{p}$, with $\mathbf{p}$ small, it becomes

$$\mathcal{G}(\mathbf{p}+\mathbf{Q}) \simeq -\frac{\rho\xi^{-2}}{\xi^{-2} + \mathbf{p}^2}, \tag{A22}$$

where ξ is the correlation length

$$\xi = \sqrt{\frac{1-\rho}{4\rho}}. \tag{A23}$$

Finally, the connected hole density correlation function (the structure factor) in real space for $\rho \to 1$ is

$$\mathcal{G}(r) = \frac{(-1)^{r_x + r_y + 1}}{\sqrt{\pi \xi r}} e^{-\xi r}. \tag{A24}$$

If we restore the units, the correlation length is $\xi = a\sqrt{\frac{1-\rho a^2}{4\rho a^2}}$.

Surprisingly, given how crude this approximation is, the result of Eq. (A24) is consistent with the numerical results provided by Krauth and Moessner[23] for much of the dimer-density range they studied. Significant deviations are seen only upon approach of the close packing regime where the classical dimer model is critical and this mean-field calculation fails, e.g., the correlation length diverges as $\rho \to 0$ with exponent 1/2, given by Eq. (A23) (the mean-field value). The correct value of the exponent can be deduced from Table I and it is $1/(2-1/4)=4/7$ (1/4 being the scaling dimension of the hole operator for the noninteracting case.) As we show in Sec. IV A (and in Table I), the dimension of the hole operator grows from the value of 1/4 for free dimers to a value of 2 at the (Kosterlitz-Thouless) transition to the columnar state, where it should exhibit an essential singularity due to the marginality of the hole operator.

2. Adding interactions between dimers

Clearly, the mean-field method for the noninteracting dimer-hole system can be easily extended to dimer-hole systems with local interactions. In the case of attractive interactions between parallel dimers, the partition function of the monomer-dimer system should be

$$\mathcal{Z}_{\text{d-int}} = \int \mathcal{D}\eta \mathcal{D}\eta^\dagger \exp\left(\sum_i \eta_i \eta_i^\dagger + \frac{z}{2}\sum_{ij} M_{ij}\eta_i \eta_i^\dagger \eta_j \eta_j^\dagger + \frac{V}{4}\sum_{ijkl} \tilde{M}_{ijkl}\eta_i \eta_i^\dagger \eta_j \eta_j^\dagger \eta_k \eta_k^\dagger \eta_l \eta_l^\dagger\right), \tag{A25}$$

where $V=z^2(e^u-1)$ for an attractive interaction of strength $u>0$ between parallel neighboring dimers. M_{ij} represents the coordination array of the lattice and it takes the value of 1 when i is nearest neighbor to j and otherwise is zero. In the same respect, $\tilde{M}_{ijkl}$ takes the value of 1 only when i,j,k,l are arranged on a square plaquette and is zero otherwise. The sums run along all possible lattice sites for each index. We may perform two Hubbard-Stratonovich transformations by introducing the fields χ and ϕ and then we have (again, dropping all normalization constants)

$$\mathcal{Z}_{\text{d-int}} = \int \mathcal{D}\eta \mathcal{D}\eta^\dagger \mathcal{D}\chi \exp\left[\sum_i \eta_i \eta_i^\dagger - \frac{1}{V}\sum_{ijkl} \chi_{ij}(\tilde{M}_{ijkl})^{-1}\chi_{kl} + \sum_{ij} \eta_i \eta_i^\dagger \eta_j \eta_j^\dagger \left(\chi_{ij} + \frac{z}{2}M_{ij}\right)\right]$$

$$= \int \mathcal{D}\eta \mathcal{D}\eta^\dagger \mathcal{D}\chi \mathcal{D}\phi \exp\left[-\frac{1}{V}\sum_{ijkl} \chi_{ij}(\tilde{M}_{ijkl})^{-1}\chi_{kl}\right.$$

$$-\frac{1}{4}\sum_i \phi_i\left(\chi_{ij}+\frac{z}{2}M_{ij}\right)^{-1}\phi_j+\sum_{ij}\eta_i\eta_i^\dagger(\phi_i+1)\Bigg]$$
$$=\int \mathcal{D}\chi\mathcal{D}\phi\exp\Bigg[-\frac{1}{V}\sum_{ijkl}\chi_{ij}(\tilde{M}_{ijkl})^{-1}\chi_{kl}$$
$$-\frac{1}{4}\sum_{ij}\phi_i\left(\chi_{ij}+\frac{z}{2}M_{ij}\right)^{-1}\phi_j+\sum_i \ln(\phi_i+1)\Bigg]. \tag{A26}$$

Just as we did above, we introduce a set of auxiliary sources J_{ij}^{χ} defined on links ij and J_i^{ϕ} defined on sites i. The partition function now reads

$$\mathcal{Z}_{\text{d-int}}[J^{\chi},J^{\phi}]=\int \mathcal{D}\chi\mathcal{D}\phi e^{-(1/Vz)\mathcal{S}(\phi,\chi;J^{\phi},J^{\chi})}, \tag{A27}$$

where the action now is

$$\mathcal{S}(\phi,\chi;J^{\phi},J^{\chi})=z\sum_{ijkl}(\chi_{ij}-J_{ij}^{\chi})(\tilde{M}_{ijkl})^{-1}(\chi_{kl}-J_{kl}^{\chi})$$
$$+\frac{Vz}{4}\sum_{ij}(\phi_i-J_i^{\phi})\left(\chi_{ij}+\frac{z}{2}M_{ij}\right)^{-1}(\phi_j-J_j^{\phi})$$
$$-Vz\sum_i \ln(\phi_i+1). \tag{A28}$$

We define the densities conjugate to the fields ϕ_i and χ_{ij} as

$$n_i=\frac{\partial \ln \mathcal{Z}_{\text{d-int}}}{\partial J_i^{\phi}}=\frac{1}{2}\sum_j(\chi_{ij}+zM_{ij})^{-1}\phi_j,$$

$$m_{ij}=\frac{\partial \ln \mathcal{Z}_{\text{d-int}}}{\partial J_{ij}^{\chi}}=\frac{2}{V}\sum_{kl}(\tilde{M}_{ijkl})^{-1}\chi_{kl}. \tag{A29}$$

Solving for the fields and replacing in Eq. (A28), we finally have the following for the effective potential or equivalently the Gibbs free energy:

$$\Gamma(z,V)=\frac{V}{4}\sum_{ijkl}m_{ij}\tilde{M}_{ijkl}m_{kl}+\sum_{ij}n_i\left(\frac{V}{2}\sum_{kl}\tilde{M}_{ijkl}m_{kl}+\frac{z}{2}M_{ij}\right)n_j$$
$$-\sum_i \ln\left[2\sum_j\left(\frac{V}{2}\sum_{kl}\tilde{M}_{ijkl}m_{kl}+\frac{z}{2}M_{ij}\right)n_j+1\right]. \tag{A30}$$

The ordered phase of dimers is expected to be a columnar one. So, for $m_{ij}=(-1)^{x_i}\delta_{i,j-\hat{x}}m+m_0$ and $n_j=n$, the free energy is

$$\frac{\Gamma(z,V)}{N}=Vm^2+2Vm_0^2+4Vm_0n^2+2zn^2$$
$$-\frac{1}{2}\ln\left(1+8n\left[V\left(\frac{m}{2}+m_0\right)+\frac{z}{2}\right]\right)$$
$$-\frac{1}{2}\ln\left(1+8n\left[V\left(-\frac{m}{2}+m_0\right)+\frac{z}{2}\right]\right). \tag{A31}$$

Now, we proceed by solving two of the three extremal (saddle-point) equations:

$$\frac{\delta\Gamma}{\delta n}=0 \quad \text{and} \quad \frac{\delta\Gamma}{\delta m_0}=0, \tag{A32}$$

which take the following explicit form:

$$8Vm_0n+4zn-\frac{4\left(V\left(\frac{m}{2}+m_0\right)+\frac{z}{2}\right)}{1+8n\left(V\left(\frac{m}{2}+m_0\right)+\frac{z}{2}\right)}$$
$$-\frac{4\left(V\left(-\frac{m}{2}+m_0\right)+\frac{z}{2}\right)}{1+8n\left(V\left(-\frac{m}{2}+m_0\right)+\frac{z}{2}\right)}=0, \tag{A33}$$

$$4Vm_0+4Vn^2-\frac{4nV}{1+8n\left(V\left(-\frac{m}{2}+m_0\right)+\frac{z}{2}\right)}$$
$$-\frac{4nV}{1+8n\left(V\left(\frac{m}{2}+m_0\right)+\frac{z}{2}\right)}=0. \tag{A34}$$

For $z=V=0$, the solution of the saddle-point equations is trivial, $m_0=n=1$. For small z, we can solve Eqs. (A33) and (A34) recursively, expanding also in the small order parameter m (this is correct close to a continuous phase transition or to a weakly first-order transition):

$$n\simeq 1-4z-8V-\frac{1}{4(2V+z)}\left(\frac{16V^2m^2}{(1+8V+4z)^2}\right.$$
$$\left.+\frac{256V^4m^4}{(1+8V+4z)^4}+\frac{4096V^6m^6}{(1+8V+4z)^6}\right), \tag{A35}$$

$$m_0\simeq\frac{2}{1+8V+4z}-1+\frac{1}{4V}\left(\frac{128V^3m^2}{(1+8V+4z)^3}+\frac{2048V^5m^4}{(1+8V+4z)^5}\right.$$
$$\left.+\frac{32768V^7m^6}{(1+8V+4z)^7}\right). \tag{A36}$$

Replacing Eqs. (A35) and (A36) in the free energy (A31), and also expanding in the small parameter z, we have

$$\frac{\Gamma(z,V)}{N}=C_0(z,V_r)+C_2(z,V_r)m^2+C_4(z,V_r)m^4+C_6(z,V_r)m^6$$
$$+\cdots, \tag{A37}$$

where $V_r\equiv\frac{V}{z^2}=e^u-1$ and

$$C_0(z,V_r)=-2z+(8-2V_r)z^2+\frac{32}{3}(-5+3V_r)z^3+O(z^4), \tag{A38}$$

$$C_2(z,V_r)=V_rz^2[1+8V_rz^2-128V_rz^3-256(-7+V_r)V_rz^4]$$
$$+O(z^7), \tag{A39}$$

$$C_4(z,V_r) = -32V_r^4 z^7(1-2(19+V_r)z+4[184+V_r(4+V_r)]z^2 + 8\{1336+V_r[-232+V_r(4+V_r)]\}z^3) + O(z^{11}), \tag{A40}$$

$$C_6(z,V_r) = 128V_r^6 z^{10}\{1-4(V_r+12)z + 4[340+V_r(28+3V_r)]z^2\} + O(z^{13}). \tag{A41}$$

In the limit of very low dimer density, $z \to 0$, from Eqs. (A38)–(A41), there is a clear first-order phase transition from an empty lattice ($n=1$, $m=0$) to a columnar dimer crystal ($m \neq 0$) because $C_2 > 0$, $C_4 < 0$, and $C_6 > 0$. In particular, in this limit, the first-order transition happens when

$$C_2 = \frac{C_4^2}{4C_6}, \tag{A42}$$

$$z^2 V_r \simeq \frac{(32V_r^4 z^7)^2}{512V_r^6 z^{10}}, \tag{A43}$$

$$e^u = 1 + \frac{1}{2z^2} \simeq \frac{1}{2}z^{-2} \Rightarrow 2z^2 e^u = 1. \tag{A44}$$

Condition (A44) can be derived through a very simple argument: In the limit of very low dimer densities, the nonlocal effects which are related to the hard-core dimer constraint are negligible. If we consider just a single plaquette, then the contribution from four holes on this plaquette to the Gibbs weight of the partition function will be just unity, but the contribution of two parallel dimers arranged either vertically or horizontally will be $2z^2e^u$. When $2z^2e^u=1$, the holes become unstable to the formation of pairs of parallel nearest neighboring dimers and the result is a columnar dimer crystal.

When $C_2=C_4=0$ (whereas C_6 remains positive), there is a mean-field tricritical point where the transition ultimately becomes continuous. Using the approximate Eqs. (A39)–(A41), we can have an estimate for the tricritical point. Solving the set of equations, we arrive at the following estimate:

$$z_{tr} = 0.075, \tag{A45}$$

$$u_{tr} = 2.733. \tag{A46}$$

Remarkably enough, these estimates are very close to the estimates from the grand-canonical simulations that are presented in Sec. V. However, we should be very cautious on taking these estimates too seriously since the terms in the expansion of the coefficients C_0, C_2, C_4, and C_6 in powers of z generically have alternating signs with increasingly large constant coefficients, which suggests that this expansion is not convergent. In any case, mean-field approximations, such as the one presented here, fail in two dimensions. The actual multicritical point has a more complex analytic structure, akin to a Kosterlitz-Thouless transition, than suggested by these Landau-Ginzburg-type arguments. On the other hand, the multicritical point can be approached from the high dimer-density limit, where the transition is continuous and thus, an effective field theory description is possible. As we show in Secs. IV A and IV B, this multicritical point is controlled by a marginally relevant operator and belongs to the Kosterlitz-Thouless universality class.

APPENDIX B: DERIVATION OF THE SINGLE MODE APPROXIMATION OSCILLATOR STRENGTH FUNCTIONS $f(\mathbf{k})$

In this appendix, we present the details of the calculations of the SMA oscillator strength functions $f(\mathbf{k})$ discussed in Sec. VII.

1. Fixed-hole-density model

a. Hole density excitations

The only term of Hamiltonian (2.6) which does not commute with the hole density operator is the hopping term for the holes. This term, in terms of destruction-creation Pauli operators $\sigma^{d^\pm}_{\hat{\alpha}}$ and $\sigma^{h^\pm}$, can be written as

$$\mathcal{T}_{\text{t-hole}} = -\tilde{t}_{\text{hole}} \sum_{\langle ijk \rangle} \sigma^{h^-}(\mathbf{r}_i)\sigma^{h^+}(\mathbf{r}_k)\sigma^{d^+}_{\hat{\alpha}}(\mathbf{r}_{ij})\sigma^{d^-}_{\hat{\alpha}}(\mathbf{r}_{jk}). \tag{B1}$$

At this point, we are not interested for the possible orientations of the dimers with respect to the holes, as the hole density operator commutes with the dimer-density operator. Now, we will repeatedly use that

$$[\sigma^{h^\pm}, \sigma^h] = \mp 2\sigma^{h^\pm} \tag{B2}$$

at the same position in real space. At any distance different from zero, the commutator vanishes. For a given hole at a position $\mathbf{R}$, there are four possible positions $\mathbf{R}' = \mathbf{R} \pm \hat{x} \pm \hat{y}$ where it may move through the available hopping term. By counting contributions from all these terms for every site of the lattice, we exactly take into account all the terms of the Hamiltonian including Hermitian conjugates.

If $\mathbf{R}$ is the initial hole position and $\mathbf{R}+\mathbf{r}_0$ the final one, then $\mathbf{r}_0$ has eight possible values: $\mathbf{r}_0 = \pm\hat{x} \pm \hat{y}$. The first commutator can now be computed for any site $\mathbf{R}$ [the operator $\mathcal{T}_{\text{hole}}(\mathbf{R},\mathbf{r}_0)$ contains each of the above eight hopping terms]. We have

$$[-t_{\text{hole}}\mathcal{T}_{\text{hole}}(\mathbf{R},\mathbf{r}_0), \sigma^h(\mathbf{k})] = -t_{\text{hole}}\mathcal{T}_{\text{hole}}(\mathbf{R},\mathbf{r}_0)(e^{-i\mathbf{k}\cdot\mathbf{R}} - e^{-i\mathbf{k}\cdot(\mathbf{R}+\mathbf{r}_0)}), \tag{B3}$$

$$[\sigma^h(-\mathbf{k}), -t_{\text{hole}}\mathcal{T}_{\text{hole}}(\mathbf{R},\mathbf{r}_0)] = t_{\text{hole}}\mathcal{T}_{\text{hole}}(\mathbf{R},\mathbf{r}_0)(e^{i\mathbf{k}\cdot\mathbf{R}} - e^{i\mathbf{k}\cdot(\mathbf{R}+\mathbf{r}_0)}), \tag{B4}$$

$$[\sigma^h(-\mathbf{k}),[-t_{\text{hole}}\mathcal{T}_{\text{hole}}(\mathbf{R},\mathbf{r}_0), \sigma^h(\mathbf{k})]] = 2t_{\text{hole}}\mathcal{T}_{\text{hole}}(\mathbf{R},\mathbf{r}_0)[1-\cos(\mathbf{k}\cdot\mathbf{r}_0)]. \tag{B5}$$

Thus, the oscillator strength $f(\mathbf{k})$ can now be calculated:

$$f(\mathbf{k}) = \sum_{\mathbf{R},\mathbf{r}_0} \langle [\sigma^h(-\mathbf{k}),[-t_{\text{hole}}\mathcal{T}_{\text{hole}}(\mathbf{R},\mathbf{r}_0), \sigma^h(\mathbf{k})]]\rangle \times 2t_{\text{hole}} \sum_{\mathbf{r}_0} [1-\cos(\mathbf{k}\cdot\mathbf{r}_0)]. \tag{B6}$$

If we set $\mathbf{k} = \mathbf{Q}_0 + \mathbf{q}$, where $\mathbf{q}$ is assumed to be small, then for

$\mathbf{Q}_0=(0,0)$, the above expression can be expanded:

$$f(\mathbf{k}) = 4t_{\text{hole}}\mathbf{q}^2. \tag{B7}$$

For $\mathbf{Q}_0=(\pi,\pi)$, we have

$$f(\mathbf{k}) = 2t_{\text{hole}}\sum_{\mathbf{r}_0}[1-(-1)^{r_{0x}+r_{0y}}\cos(\mathbf{q}\cdot\mathbf{r}_0)]. \tag{B8}$$

$r_{0x}+r_{0y}$ can take only the values of 0 and 2. Thus, $(-1)^{r_{0x}+r_{0y}}=1$ for all $\mathbf{r}_0$'s. In this way, if we expand around (π,π), we have again

$$f(\mathbf{k}) = 4t_{\text{hole}}\mathbf{q}^2. \tag{B9}$$

It is obvious that for any other $\mathbf{k}$'s, the oscillator strength $f(\mathbf{k})$ cannot vanish. So, the upper bound to the excitation energy for the holes is

$$E_{\mathbf{k}} - E_0 \leqslant \frac{f(\mathbf{k})}{s(\mathbf{k})}. \tag{B10}$$

b. Dimer density excitations

In the same way as before, we may calculate the numerator for the case where we use the dimer density operator $\sigma^d_{\hat{\alpha}}$ instead of the hole density. Now, the operator does not commute with both the dimer-flip term and the hole-hopping terms.

In the case of the dimer-flip term, the commutator will give the following contribution[1,86] (the dimer-density operator is taken to be at the $\hat{\alpha}=\hat{x}$ direction):

$$f_{\text{dimer-flip}}(\mathbf{k}) = 8t\sum_{\mathbf{r}=\pm y}[1+\cos(\mathbf{k}\cdot\mathbf{r}_0)], \tag{B11}$$

where $r_0=\pm\hat{y}$ for the case of a horizontal dimer. This term comes from the original quantum dimer model. As it was pointed out in Ref. 86, it vanishes quadratically at $Q_0=(\pi,\pi)$ and $Q_1=(0,\pi)$. In particular, at $Q_0=(\pi,\pi)$, with $\mathbf{k}=\mathbf{Q}_0+\mathbf{q}$, it vanishes as

$$f_{\text{dimer-flip}}(\mathbf{q}) = 8tq^2. \tag{B12}$$

In the case of hole-hopping terms which mix horizontal and vertical dimers $\mathbf{r}_0'=-\mathbf{r}_0/2=(\pm\hat{x}\pm\hat{y})/2$ (where $\mathbf{r}_0$ denotes the displacement vector for the hole in the considered move), we have

$$[-t_{\text{hole}}\mathcal{T}^{(1)}_{\text{hole}}(\mathbf{R},\mathbf{r}_0),\sigma^d_{\hat{x}}(\mathbf{k})] = -t_{\text{hole}}\mathcal{T}^{(1)}_{\text{hole}}(\mathbf{R},\mathbf{r}_0)(e^{-i\mathbf{k}\cdot(\mathbf{R}+\mathbf{r}_0/2)}-e^{-i\mathbf{k}\cdot\mathbf{R}}), \tag{B13}$$

$$[\sigma^d_{\hat{x}}(-\mathbf{k}),[-t_{\text{hole}}\mathcal{T}^{(1)}_{\text{hole}}(\mathbf{R},\mathbf{r}_0),\sigma^d_{\hat{x}}(\mathbf{k})]] = 2t_{\text{hole}}\mathcal{T}^{(1)}_{\text{hole}}(\mathbf{R},\mathbf{r}_0)[1-\cos(\mathbf{k}\cdot\mathbf{r}_0/2)], \tag{B14}$$

$$f_{\text{hole}(1)}(\mathbf{k}) = 2t_{\text{hole}}\sum_{\mathbf{r}_0}\left[1-\cos\left(\frac{\mathbf{k}\cdot\mathbf{r}_0}{2}\right)\right]. \tag{B15}$$

2. Fixed-hole fugacity model

Let us follow the same strategy as before ($\mathbf{r}_0=\hat{x},\hat{y}$):

$$[-\tilde{t}_{\text{hole}}\mathcal{T}^{(2)}_{\text{hole}}(\mathbf{R},\mathbf{r}_0),\sigma^h(\mathbf{k})] = \tilde{t}_{\text{hole}}\mathcal{T}^{(2)}_{\text{hole}}(\mathbf{R},\mathbf{r}_0)(e^{-i\mathbf{k}\cdot\mathbf{R}}+e^{-i\mathbf{k}\cdot(\mathbf{R}+\mathbf{r}_0)}), \tag{B16}$$

where $\mathcal{T}^{(2)}_{\text{hole}}$ denotes the resonance part of the Hamiltonian in Eq. (2.8). We also have

$$[\sigma^h(-\mathbf{k}),[-\tilde{t}_{\text{hole}}\mathcal{T}^{(2)}_{\text{hole}}(\mathbf{R},\mathbf{r}_0),\sigma^h(\mathbf{k})]] = 2\tilde{t}_{\text{hole}}\mathcal{T}^{(2)}_{\text{hole}}(\mathbf{R},\mathbf{r}_0)[1+\cos(\mathbf{k}\cdot\mathbf{r}_0)]. \tag{B17}$$

Finally, after adding the contribution of the Hermitian conjugate part of the Hamiltonian, we have

$$f_{\text{hole}(2)}(\mathbf{k}) = 4t_{\text{pairing}}[2+\cos(\mathbf{k}_x)+\cos(\mathbf{k}_y)]. \tag{B18}$$

[1] D. S. Rokhsar and S. A. Kivelson, Phys. Rev. Lett. **61**, 2376 (1988).
[2] P. W. Anderson, Science **235**, 1196 (1987).
[3] S. A. Kivelson, D. S. Rokhsar, and J. Sethna, Phys. Rev. B **35**, 8865 (1987).
[4] E. Fradkin, *Field Theories of Condensed Matter Systems* (Addison-Wesley, Redwood City, CA, 1991), Chap. 6.
[5] N. Read and S. Sachdev, Phys. Rev. Lett. **66**, 1773 (1991).
[6] S. Sachdev and N. Read, Int. J. Mod. Phys. B **5**, 219 (1991).
[7] R. Moessner and S. L. Sondhi, Phys. Rev. Lett. **86**, 1881 (2001).
[8] R. Moessner, S. L. Sondhi, and E. Fradkin, Phys. Rev. B **65**, 024504 (2001).
[9] E. Fradkin, D. A. Huse, R. Moessner, V. Oganesyan, and S. L. Sondhi, Phys. Rev. B **69**, 224415 (2004).
[10] A. Vishwanath, L. Balents, and T. Senthil, Phys. Rev. B **69**, 224416 (2004).
[11] E. Ardonne, P. Fendley, and E. Fradkin, Ann. Phys. (N.Y.) **310**, 493 (2004).
[12] E. Fradkin and S. A. Kivelson, Mod. Phys. Lett. B **4**, 225 (1990).
[13] L. Balents, L. Bartosch, A. Burkov, S. Sachdev, and K. Sengupta, Phys. Rev. B **71**, 144509 (2005).
[14] F. Alet, J. L. Jacobsen, G. Misguich, V. Pasquier, F. Mila, and M. Troyer, Phys. Rev. Lett. **94**, 235702 (2005).
[15] O. F. Syljuasen, Phys. Rev. B **71**, 020401(R) (2005).
[16] F. Alet, Y. Ikhlef, J. L. Jacobsen, G. Misguich, and V. Pasquier, Phys. Rev. E **74**, 041124 (2006).
[17] C. Castelnovo, C. Chamon, C. Mudry, and P. Pujol, Ann. Phys. (N.Y.) **322**, 903 (2007).
[18] D. Poilblanc, F. Alet, F. Becca, A. Ralko, F. Trousselet, and F. Mila, Phys. Rev. B **74**, 014437 (2006).
[19] L. P. Kadanoff, Phys. Rev. Lett. **39**, 903 (1977).
[20] P. Ginsparg, in *Champs, Cordes et Phénomènes Critiques/ Fields, Strings and Critical Phenomena*, edited by E. Brézin and J. Zinn-Justin (Elsevier Science, New York, 1989).
[21] D. Boyanovsky, J. Phys. A **22**, 2601 (1989).
[22] P. Lecheminant, A. O. Gogolin, and A. N. Nersesyan, Nucl. Phys.

B **639**, 502 (2002).
[23] W. Krauth and R. Moessner, Phys. Rev. B **67**, 064503 (2003).
[24] J. Liu and E. Luijten, Phys. Rev. Lett. **92**, 035504 (2004).
[25] P. Fendley, R. Moessner, and S. L. Sondhi, Phys. Rev. B **66**, 214513 (2002).
[26] F. Trousselet, P. Pujol, F. Alet, and D. Poilblanc, arXiv:0705.1550 (unpublished).
[27] R. J. Baxter, J. Phys. C **6**, L94 (1973).
[28] N. Read and S. Sachdev, Phys. Rev. Lett. **62**, 1694 (1989).
[29] K. S. Raman, R. Moessner, and S. L. Sondhi, Phys. Rev. B **72**, 064413 (2005).
[30] C. Castelnovo, C. Chamon, C. Mudry, and P. Pujol, Ann. Phys. (N.Y.) **318**, 316 (2005).
[31] S. Samuel, J. Math. Phys. **21**, 2806 (1980).
[32] S. Samuel, J. Math. Phys. **21**, 2820 (1980).
[33] H. W. J. Blöte and H. J. Hilhorst, J. Phys. A **15**, L631 (1982).
[34] H. W. J. Blöte and M. P. Nightingale, Physica A **112**, 405 (1982).
[35] C. L. Henley, J. Stat. Phys. **89**, 483 (1997).
[36] L. S. Levitov, Phys. Rev. Lett. **64**, 92 (1990).
[37] W. Zheng and S. Sachdev, Phys. Rev. B **40**, 2704 (1989).
[38] R. Moessner and S. L. Sondhi, Phys. Rev. B **68**, 054405 (2003).
[39] G. Forgacs and E. Fradkin, Phys. Rev. B **23**, 3442 (1981).
[40] M. E. Fisher and J. Stephenson, Phys. Rev. **132**, 1411 (1963).
[41] R. Youngblood, J. D. Axe, and B. M. McCoy, Phys. Rev. B **21**, 5212 (1980).
[42] J. K. Kondev and C. L. Henley, Nucl. Phys. B **464**, 540 (1996).
[43] L. P. Kadanoff and H. Ceva, Phys. Rev. B **3**, 3918 (1971).
[44] E. Fradkin and L. P. Kadanoff, Nucl. Phys. B **170**, 1 (1980).
[45] A. B. Zamolodchikov and V. A. Fateev, Sov. Phys. JETP **62**, 215 (1985).
[46] E. Witten, Nucl. Phys. B **142**, 285 (1978).
[47] L. P. Kadanoff and A. C. Brown, Ann. Phys. (N.Y.) **121**, 318 (1979).
[48] J. M. Kosterlitz and D. J. Thouless, J. Phys. C **6**, 1181 (1973).
[49] J. M. Kosterlitz, J. Phys. C **7**, 1046 (1974).
[50] J. V. José, L. P. Kadanoff, S. Kirkpatrick, and D. R. Nelson, Phys. Rev. B **16**, 1217 (1977).
[51] A. Luther and I. Peschel, Phys. Rev. B **12**, 3908 (1975).
[52] P. B. Wiegmann, J. Phys. C **11**, 1583 (1978).
[53] D. J. Amit, Y. Y. Goldschmidt, and G. Grinstein, J. Phys. A **13**, 585 (1980).
[54] M. P. M. den Nijs, Phys. Rev. B **23**, 6111 (1981).
[55] L. P. Kadanoff, J. Phys. A **7**, 1399 (1978).
[56] B. Nienhuis, in *Phase Transitions and Critical Phenomena*, edited by C. Domb and J. Lebowitz (Academic, London, 1987), Vol. 11, p. 1.
[57] P. Di Francesco, P. Mathieu, and D. Sénéchal, *Conformal Field Theory* (Springer-Verlag, New York, 1997).
[58] E. Witten, Commun. Math. Phys. **92**, 455 (1984).
[59] M. Kohmoto, M. den Nijs, and L. P. Kadanoff, Phys. Rev. B **24**, 5229 (1981).
[60] V. J. Emery, in *Highly Conducting One-Dimensional Solids*, edited by J. T. Devreese, R. P. Evrard, and V. E. van Doren (Plenum, New York, 1979), p. 327, and references therein.
[61] B. Nienhuis and M. Nauenberg, Phys. Rev. B **13**, 2021 (1976).
[62] A. D. Bruce and A. Aharony, Phys. Rev. B **11**, 478 (1975).
[63] E. Fradkin and J. E. Hirsch, Phys. Rev. B **27**, 1680 (1983).
[64] G. S. Grest and M. Widom, Phys. Rev. B **24**, 6508 (1981).
[65] E. Fradkin, Phys. Rev. Lett. **53**, 1967 (1984).
[66] J. L. Cardy, M. Nauenberg, and D. J. Scalapino, Phys. Rev. B **22**, 2560 (1980).
[67] J. Liu and E. Luijten, Phys. Rev. E **71**, 066701 (2005).
[68] K. Binder, Z. Phys. B: Condens. Matter **43**, 119 (1981).
[69] A. M. Ferrenberg and R. H. Swendsen, Phys. Rev. Lett. **63**, 1195 (1989).
[70] Y. C. Kim, M. E. Fisher, and E. Luijten, Phys. Rev. Lett. **91**, 065701 (2003).
[71] V. I. Pokrovsky and A. L. Talapov, Sov. Phys. JETP **75**, 1151 (1978).
[72] P. Bak, Rep. Prog. Phys. **45**, 587 (1982).
[73] M. E. Fisher and W. Selke, Phys. Rev. Lett. **44**, 1502 (1980).
[74] S. Papanikolaou, K. S. Raman, and E. Fradkin, Phys. Rev. B **75**, 094406 (2007).
[75] R. P. Feynman, *Statistical Mechanics* (Benjamin, New York, 1972).
[76] G. D. Mahan, *Many Particle Physics* (Plenum, New York, 1990).
[77] D. P. Arovas and S. M. Girvin, Lectures presented at the Seventh International Conference on Recent Progress in Many Body Theories, Minneapolis, MN, 1991 (unpublished).
[78] S. M. Girvin, A. H. MacDonald, and P. M. Platzman, Phys. Rev. Lett. **54**, 581 (1985).
[79] D. P. Arovas, A. Auerbach, and F. D. M. Haldane, Phys. Rev. Lett. **60**, 531 (1988).
[80] J. Zaanen and O. Gunnarsson, Phys. Rev. B **40**, 7391 (1989).
[81] S. A. Kivelson and V. J. Emery, in *Strongly Correlated Electron Materials: The Los Alamos Symposium 1993*, edited by K. Bedell, Z. Wang, D. E. Meltzer, A. V. Balatsky, and E. Abrahams (Addison-Wesley, Redwood City, CA, 1994), pp. 619–650.
[82] S. A. Kivelson, E. Fradkin, and V. J. Emery, Nature (London) **393**, 550 (1998).
[83] V. J. Emery, S. A. Kivelson, and J. M. Tranquada, Proc. Natl. Acad. Sci. U.S.A. **96**, 8814 (1999).
[84] S. Sachdev, Rev. Mod. Phys. **75**, 913 (2003).
[85] O. J. Heilmann and E. H. Lieb, Phys. Rev. Lett. **24**, 1412 (1970).
[86] R. Moessner and S. L. Sondhi, Phys. Rev. B **68**, 184512 (2003).